Geochemistry Geophysics Geosystems G3
AN ELECTRONIC JOURNAL OF THE EARTH SCIENCES
Published by AGU and the Geochemical Society

Article
Volume 10, Number 9
25 September 2009
Q09007, doi:10.1029/2009GC002373
ISSN: 1525-2027

Constraints on asthenospheric flow from the depths of oceanic spreading centers: The East Pacific Rise and the Australian-Antarctic Discordance

W. Roger Buck, Christopher Small, and William B. F. Ryan

Lamont-Doherty Earth Observatory, Earth Institute at Columbia University, Palisades, New York 10964, USA (buck@ldeo.columbia.edu)

[1] The fastest spreading center, the East Pacific Rise (EPR), is consistently deeper than most other spreading centers. Its average depth along the ~5000 km length is ~3100 m, while the mean depth along the adjacent, slower spreading Pacific-Antarctic Rise (PAR) is ~2700 m. The deepest spreading center is the ~4000 m deep, ~1000 km long Australian Antarctic Discordance (AAD). Analytic and numerical models show that dynamic thinning of asthenosphere can explain the magnitude and wavelength of the depth anomalies along the EPR and AAD. Previous models did not show such significant depth anomalies along spreading centers because the equations used to describe flow of thin viscous asthenosphere were linearized. At the EPR, fast plate divergence thins the asthenosphere by both sequestering it into diverging lithosphere and dragging it with the plates in contrast to the slower spreading but faster migrating PAR. The AAD asthenosphere is starved because of the restriction of asthenospheric flow due to nearby thick continental lithospheric roots combined with a moderately fast spreading rate. A narrow range of asthenospheric properties explains observed depth anomalies for both the AAD and EPR. If the asthenosphere is ~100°C hotter, and so ~10 kg/m^3 less dense than the underlying asthenosphere, then the model requires an average asthenospheric thickness of ~250 km and a viscosity of ~10^{19} Pa s. Thinner asthenosphere works in the model if it has a lower density and lower viscosity. Although the source of the asthenosphere is not critical to our models, we assume that it is supplied by upwelling of depleted mantle plumes in contrast to enriched plumes that feed oceanic island basalts.

Components: 11,899 words, 11 figures, 1 table.

Keywords: asthenosphere; spreading centers.

Index Terms: 8121 Tectonophysics: Dynamics: convection currents, and mantle plumes; 8120 Tectonophysics: Dynamics of lithosphere and mantle: general (1213); 7208 Seismology: Mantle (1212, 1213, 8124).

Received 5 January 2009; **Revised** 6 May 2009; **Accepted** 1 July 2009; **Published** 25 September 2009.

Buck, W. R., C. Small, and W. B. F. Ryan (2009), Constraints on asthenospheric flow from the depths of oceanic spreading centers: The East Pacific Rise and the Australian-Antarctic Discordance, *Geochem. Geophys. Geosyst.*, *10*, Q09007, doi:10.1029/2009GC002373.

1. Introduction

[2] The depth of spreading centers gives a direct window on mantle dynamics. The small magnitude of lithospheric and crustal thickness changes along most spreading centers means that variations in the depth of those centers depend on active mantle processes. There is disagreement

about whether those depth variations reflect processes in the deep or the shallow mantle [e.g., *Davies*, 1999]. Shallower-than-normal ridges such as the Reykjanes Ridge have typically been explained in terms of shallow density anomalies. Specifically, it is thought that plume-fed hot mantle ponds below the lithosphere and buoys up the surface [e.g., *Vogt*, 1971, 1976; *Sleep*, 1996; *Ito et al.*, 1996; *Yale and Phipps Morgan*, 1998; *Albers and Christensen*, 2001; *Ribe and Christensen*, 1994]. In contrast, the extremely deep Australian-Antarctic Discordance (AAD) spreading center has been explained in terms of deep mantle flow. For the AAD either old, dense subducted slabs in the middle of the mantle pull down the surface [e.g., *Gurnis et al.*, 1998] or a cold mantle anomaly is pulled up between the thick plates of the rifting continents [*Lin et al.*, 2002].

[3] Depth variations along the deeper-than-normal East Pacific Rise are not easily fit by a density anomaly in the deep mantle. As shown by *Small and Danyushevsky* [2003] there is an abrupt step-like decrease in ridge depth between the East Pacific Rise (EPR) and the Pacific-Antarctic Ridge (PAR). The short wavelength of the change in depth combined with the relative constancy of the EPR and PAR spreading center depths over thousands of kilometers and the correspondence of the depth discontinuity to a plate kinematic discontinuity led *Small and Danyushevsky* [2003] to suggest that the transition was due to shallow mantle processes. Specifically, they asserted that variations in spreading rate and migration velocity should influence asthenospheric flux and consumption at the spreading center.

[4] In this paper we show that simple models of shallow, asthenospheric flow driven by plate motions can explain the pattern of depth variations observed around deeper-than- normal ridges [*Buck et al.*, 2003; *Ryan et al.*, 2003]. We first give a summary of ideas about how asthenosphere could be hotter than deeper mantle. Next, we describe the observations from the EPR that inspired this study. The model equations used to describe flow of a thin layer of viscous asthenosphere floating on denser mantle are derived. In Appendix A we describe analytic solutions to the derived flow equation and compare the results to the simplified approach of previous model studies. Finally, we describe observations from the AAD and show that models with the same properties used to fit the EPR data can explain the major features of the AAD.

2. Hot Asthenosphere

[5] As part of the concept of mantle plumes, *Morgan* [1971, 1972a, 1972b] proposed that the asthenosphere has a higher temperature than underlying mantle. Morgan pointed out that the upward rise of hot, buoyant mantle plumes might explain both the broad topographic swells and the basaltic outpourings of "hot spots." According to his "plume-fed asthenosphere idea, plumes would "feed" the asthenosphere and set its temperature according to the temperature of the plume source area, which Morgan took to be near the core mantle boundary. The recycling of cold lithospheric plates, or plate-scale convection, would set the temperature of the bulk of the mantle, here termed the mesosphere.

[6] Many observations have lent credence to the existence of plumes (see overviews by *Courtillot et al.* [2003] and *Sleep* [2006]). The slow motion of hot spot locations relative to each other has lead to the idea that the bulk of the mantle is very slow moving [e.g., *Stock and Molnar*, 1983; *Molnar and Stock*, 1987; *Müller et al.*, 1993]. Giant quasi-spherical heads at the top of nascent plumes are often invoked as the explanation of large igneous provinces [e.g., *Campbell and Griffiths*, 1990] and may lead to continental breakup [e.g., *Hill*, 1991]. The plume concept has become so widely accepted that it has produced a fervent antiplume backlash [e.g., *Foulger and Anderson*, 2005].

[7] Compared to plumes, the "plume-fed asthenosphere" hypothesis has not stirred as much interest. Several papers have considered possible observable effects of plume-fed asthenosphere, particularly focusing on the relation between seafloor depth and the age of oceanic lithosphere. *Phipps Morgan and Smith* [1992] and *Phipps Morgan et al.* [1995] showed that interaction of a thin asthenospheric layer with moving lithospheric plates could explain some observed variations in the depth-age and geoid-age relations. However, there are reasonable alternative explanations to account for variations in the oceanic depth-age and geoid-age relations. Small-scale convection [e.g., *Richter and Parsons*, 1975; *Haxby and Weissel*, 1986; *Buck and Parmentier*, 1986; *Huang and Zhong*, 2005] and the heating of old lithosphere by mantle plumes [e.g., *Crough*, 1978; *Detrick and Crough*,

1978], or superplumes [*McNutt*, 1998] are the most the widely discussed ways to alter the oceanic lithosphere thermal structure and so alter the seafloor depths and geoid heights. We believe that anomalously deep sections of spreading centers may give fairly direct evidence that the shallow mantle asthenosphere is less dense, and presumably hotter than the deeper mantle.

3. East Pacific Rise

[8] The EPR is the fastest spreading branch of the global mid-ocean ridge system, with spreading rates up to 16 cm/a [e.g., *Gripp and Gordon*, 1990; *Demets et al.*, 1994]. It is also deeper than most spreading centers including the adjacent slower spreading Pacific-Antarctic Ridge (PAR) as shown by *Small and Danyushevsky* [2003] (Figure 1). The only shallow portion of the EPR is in the vicinity of the major Easter hot spot [*Kingsley and Schilling*, 1998].

[9] The crustal thickness along the EPR is not significantly different from the global average for oceanic crust [*Chen*, 1992]. Thus, thin crust cannot account for the greater depth of the EPR. Any model for the depth discontinuity must explain the relative uniformity of the ridge depths on both the EPR and PAR for distances greater than the thickness of the mantle combined with a short-wavelength transition in ridge depths. A deep mantle density anomaly would necessarily produce a long-wavelength variation in the depth of the active spreading center.

[10] To our knowledge, there are no previous quantitative models to explain the ~5,000 km long section of deeper-than-normal mid-ocean ridge seen along the EPR. *Small and Danyushevsky* [2003] proposed a conceptual model in which the asthenosphere under the EPR could be thinned by increased asthenospheric consumption resulting from a combination of plate divergence and spreading center migration with respect to the lower mantle. Because the fast spreading, slowly migrating EPR converts more asthenosphere into lithosphere per unit time than the rapidly migrating, slower spreading PAR, the depth discontinuity could result from differences in asthenospheric depletion between the two spreading centers. Where the low-density asthenosphere is thinner the corresponding seafloor depth should be greater. *Small and Danyushevsky* [2003] do not define where the asthenosphere comes from or how it flows so they could not predict how much spreading center divergence and migration rates would affect asthenospheric thickness. In this paper we adopt the idea that the asthenosphere is fed by plumes and develop a quantitative model to test whether observed variations in plate motions could produce observed depth variations.

3.1. Conceptual Model

[11] A vertical cross section of suboceanic mantle illustrating plate-driven asthenospheric flow is shown in Figure 2. The asthenosphere floats on slightly denser mantle mesosphere and is overlain by much denser lithosphere. Rigid lithospheric plates diverge at a spreading center, with subduction zones located on both sides of a model ocean basin. The plate motion drags the asthenosphere away from the spreading center and toward the subduction zones where it is trapped by the curtain of subducting plates. The asthenosphere must be less dense than the mesosphere. If the asthenosphere is 100°C hotter than the mesosphere then it will have a density that is lower by about 10 kg/m^3, assuming a thermal expansion coefficient $\alpha = 3 \times 10^{-5}$°C^{-1}. It is not critical whether the mesosphere beneath the asthenosphere moves laterally with the asthenosphere as we demonstrate below.

[12] For the model cases presented here the asthenosphere is converted into lithosphere at the spreading axis. We also tested the effect of gradual conversion of asthenosphere to lithosphere and it did not qualitatively affect the results. The justification for the asthenospheric sequestration being close to the axis is that pressure release partial melting of asthenosphere upwelling beneath the axis may dry the asthenosphere and produce an increase in asthenospheric viscosity [*Hirth and Kohlstedt*, 1996; *Phipps Morgan*, 1997] sufficient for it to move with the overlying plate. To avoid cumulative thinning of the asthenosphere with time we assume a uniformly distributed influx of new asthenosphere. Precisely from what depth hot mantle upwells into the asthenosphere is not directly relevant to the model results.

3.2. Equations for Asthenospheric Flow

[13] Consider a channel of asthenosphere with a thickness h, viscosity μ and with a density that is lower than the underlying mantle by $\Delta\rho$. As long as the channel is thin compared to its lateral extent then we may use the thin layer approximation [e.g., *Batchelor*, 1967]. Then pressure P can be taken to

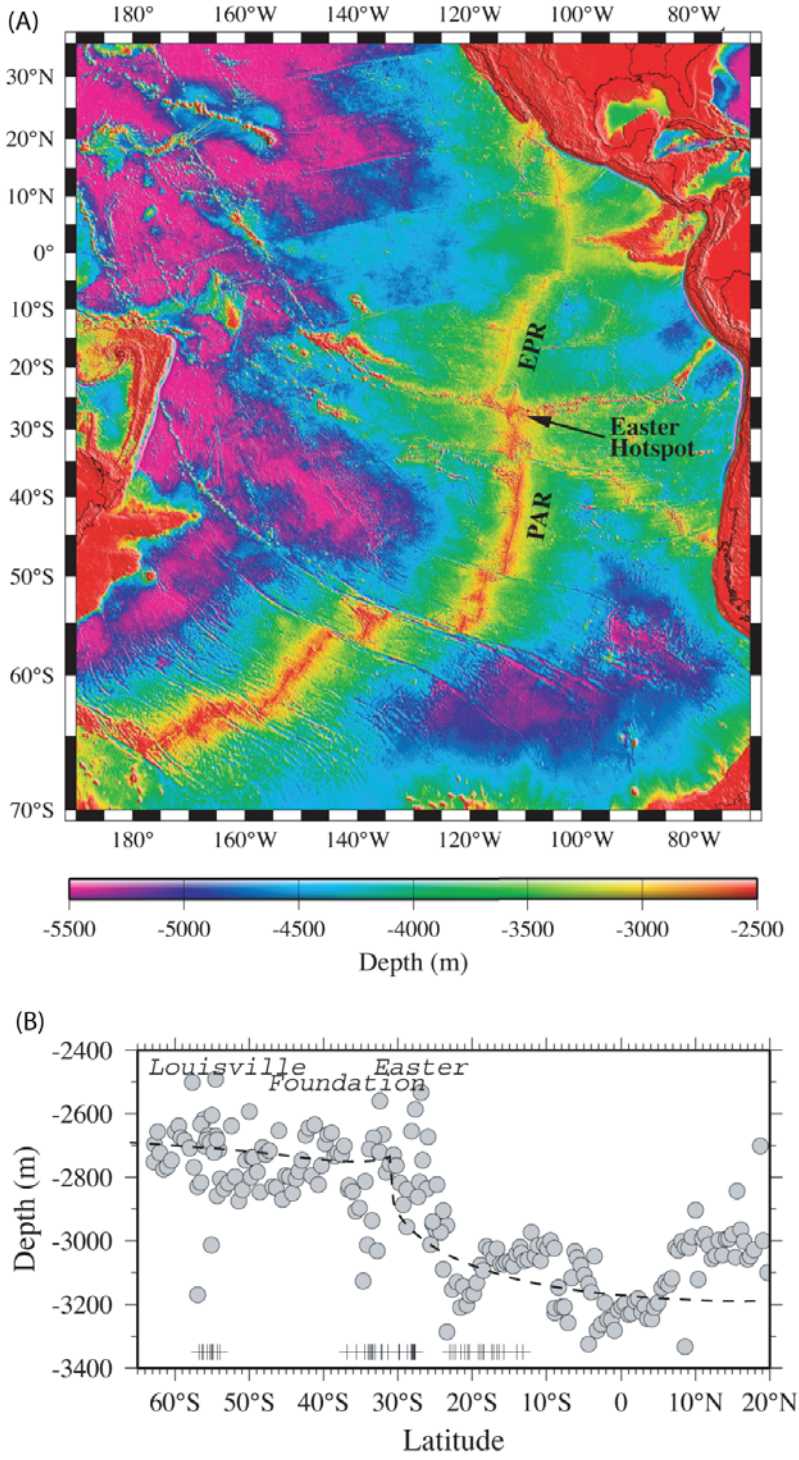

Figure 1. (a) Shaded relief bathymetry of the Pacific showing the East Pacific Rise and the Pacific Antarctic Ridge [from *Small and Danyushevsky*, 2003]. Note that the EPR is consistently deeper than the PAR. (b) Average depth within 50 km of the ridge axis along the PAR, roughly south of Easter, and the EPR [from *Small and Danyushevsky*, 2003]. Dashed line shows predicted axial depth variations for model experiments described in section 3.5.

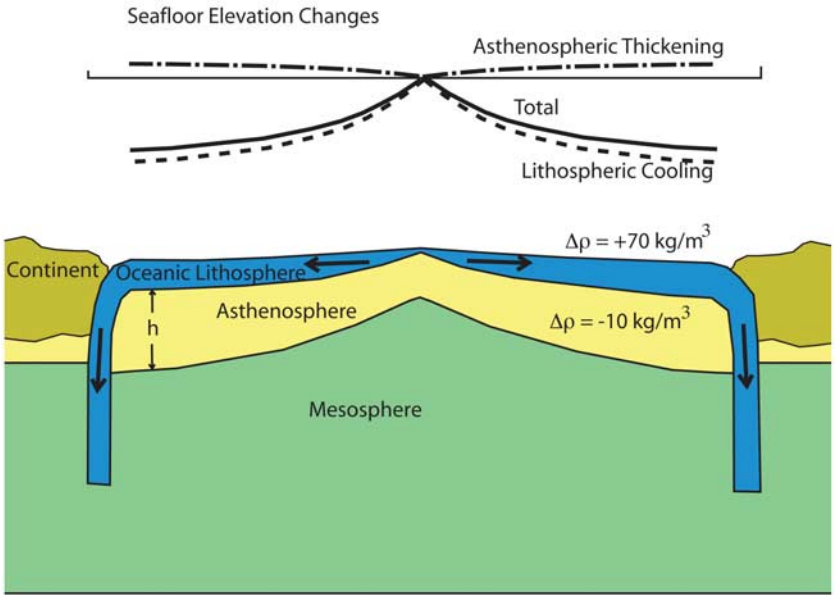

Figure 2. Schematic model cross section showing suboceanic asthenospheric thickness variations caused by the motion of lithospheric plates. The asthenosphere has a lower density than underlying mantle mesosphere and is thinned under the site of plate spreading and lithospheric accretion. The oceanic lithosphere is denser than the mesosphere, and representative density contrasts are shown. Changes of seafloor depth due to lithospheric and asthenospheric thickening away from the spreading center are shown at the top.

be uniform in the vertical, z direction, and momentum conservation implies:

$$\frac{\partial}{\partial z}\left(\mu\frac{\partial \vec{u}}{\partial z}\right) = \nabla P \tag{1}$$

where $\vec{u}$ is the horizontal velocity vector and $\nabla = (\partial/\partial x)i + (\partial/\partial y)j$ where i and j are unit vectors in the x and y directions, respectively. The top of the viscous layer is taken to be the base of a lithospheric plate which moves in the x direction with a plate velocity u_P and is free to move vertically in response to pressure changes in the lithosphere. Following most treatments of asthenospheric flow [e.g., *Schubert and Turcotte*, 1972; *Chase*, 1979; *Parmentier and Oliver*, 1979; *Phipps Morgan et al.*, 1995] we fix the base to have zero horizontal velocity.

[14] For a basal horizontal velocity of zero and a surface horizontal velocity of u_p in the x direction the components of the horizontal velocity of the asthensophere are:

$$\begin{aligned} u_x &= \frac{\left(\partial P/\partial x\right)}{2\mu}\left(z^2 - hz\right) + \frac{u_p z}{h} \\ u_y &= \frac{\left(\partial P/\partial y\right)}{2\mu}\left(z^2 - hz\right) \end{aligned} \tag{2}$$

Integrating the velocity components over the thickness of the asthenosphere gives the components of asthenospheric flux:

$$\begin{aligned} q_x &= \frac{-h^3\left(\partial P/\partial x\right)}{12\mu} + \frac{u_p h}{2} \\ q_y &= \frac{-h^3\left(\partial P/\partial y\right)}{12\mu} \end{aligned} \tag{3}$$

If the lithosphere lies below water of density ρ_W then pressure variations in asthenosphere with a density ρ_A are related to deflections of the lithospheric surface (or water depth), d, as:

$$\nabla P = -g(\rho_A - \rho_W)\nabla d \tag{4}$$

where g is the acceleration of gravity.

[15] To understand the distribution of asthenospheric thickness and how it relates to asthenospheric pressure gradients we have to specify how the layer base (the asthenosphere-mesosphere boundary) responds to pressure variations. Plate motions and any resulting pressure variations in the asthenosphere are relatively stable over periods of ~10 Ma. Therefore the loads of asthenospheric

thickness variations should produce an effectively local isostatic response in the mesosphere giving:

$$\nabla d = -\frac{(\rho_M - \rho_A)}{(\rho_M - \rho_W)}\nabla h, \tag{5}$$

where ρ_M is the density of the mesosphere.

[16] This assumption is different from that made by most previous workers on asthenospheric flow [e.g., *Parmentier and Oliver*, 1979; *Yale and Phipps Morgan*, 1998] who consider a rigid mesosphere. To the extent that mesosphere deformation can be treated in terms of flow in a viscous half-space, as in simple glacial rebound models [e.g., *Turcotte and Schubert*, 2002] then we would expect a fairly short time of response compared to the 10 Ma time scale of spreading center migration. In section 3.3, we formally estimate the response time to asthenospheric loading of the mesosphere and show that the present assumption is reasonable.

[17] Deflections of the base of the isostatically floating asthenosphere change the vertical stress by $g\rho_M$. Then pressure gradients can be simply related to layer thickness gradients as:

$$\nabla P = g\Delta\rho^*\nabla h \tag{6}$$

where

$$\Delta\rho^* = {}^{(\rho_A-\rho_W)(\rho_M-\rho_A)}/_{(\rho_M-\rho_W)}.$$

[18] Flow in the channel is driven by motion of overlying lithospheric plates moving with a horizontal velocity u_p and by distributed sources and sinks S. Both u_p and S can vary in the horizontal x, y plane. At a given position the change in asthenospheric layer thickness with time equals the sum of lateral gradients in asthenospheric fluxes plus any sources and sinks, given by:

$$\frac{\partial h}{\partial t} = \nabla\cdot\vec{q} + S$$

or

$$\frac{\partial h}{\partial t} = -\frac{\partial}{\partial x}\left(\frac{\Delta\rho^* g h^3}{12\mu}\frac{\partial h}{\partial x} - \frac{u_p h}{2}\right) - \frac{\partial}{\partial y}\left(\frac{\Delta\rho^* g h^3}{12\mu}\frac{\partial h}{\partial y}\right) + S. \tag{7}$$

This is essentially the same equation used to model lower crustal flow in the thin layer, isostatic limit [e.g., *Bird*, 1991; *Buck*, 1991, 1992]. This thin sheet description is very similar to the approach used to model ice sheet flow [e.g., *Paterson*, 1994].

[19] Once we solve for asthenospheric thickness variations we can calculate the related dynamic ocean depth variations, $d(x, y)$. The dynamic depth is taken to be zero where the asthenospheric thickness equals the average value h_a, so that:

$$d = d_{\max}(1 - h/h_a)$$

where

$$d_{\max} = \frac{(\rho_M - \rho_A)}{(\rho_M - \rho_W)}h_a. \tag{8}$$

[20] Equation (7) can be expressed in terms of the following nondimensional variables: $x' = x/h_a$, $y' = y/h_a$, $h' = h/h_a$, $t' = t^*u_0h_a$, $u_p' = u_p/u_0$, and $S' = S/u_0h_a$ u_0h_a giving:

$$\frac{\partial h'}{\partial t'} = -\frac{\partial}{\partial x'}\left(Rm\frac{\partial h'}{\partial x'} - \frac{\mu_p'}{2}\right) - \frac{\partial}{\partial y'}\left(Rm\frac{\partial h'}{\partial y'}\right) + S' \tag{9}$$

showing that an important parameter is the dimensionless Ramberg number:

$$Rm = \frac{\Delta\rho^* g h_a^2}{\mu u_0}. \tag{10}$$

The Ramberg number is a measure of the ratio of gravitational stresses to shear stresses [e.g., *Medvedev*, 2002]. Table 1 gives definitions of the coordinates, parameters and variables that describe this problem.

3.3. Treatment of "1-D" Asthenospheric Flow

[21] Before describing models that treat 3-D regions of flow variation, it is useful to investigate simpler cases. If boundary conditions and sources can be taken to be uniform in one horizontal direction, say the y direction, then a one-dimensional version of equation (7) holds, with variations of h only in the x direction. To solve this equation we use a standard explicit finite difference approximation with a uniform spatial grid and a Courant condition to choose a time step.

[22] Numerical solutions to a 1-D version of equation (7) allow us to consider how model parameters and ridge migration might affect asthenospheric thickness and seafloor depth. Figure 3 shows results of 1-D channel flow calculations for a 10,000 km wide model spreading system with an asthenospheric viscosity of 10^{19} Pa s. The axis of spreading is a sink for all the 100 km of asthenosphere assumed to cool to form the lithosphere and

Table 1. Parameters and Variables

Parameter or Variable	Definition
	Defined Parameters
x	horizontal distance parallel to the plate spreading direction (m)
y	horizontal distance perpendicular to the plate spreading direction (m)
z	depth in asthenosphere (m)
t	time (s)
g	acceleration of gravity
ρ_A, ρ_M, ρ_W	densities of asthenosphere, mesosphere and water, respectively (kg/m^3)
h(x, y)	thickness of asthenosphere (m)
d(x, y)	seafloor depth anomaly due to asthenosphere thickness variations (m)
u_x, u_y	components of horizontal asthenospheric velocity (m/s)
q_x, q_y	components of horizontal asthenospheric flux (m^2/s)
	Model Variables
μ	viscosity of asthenosphere (Pa s)
h_a	average thickness of asthenosphere (m)
$\Delta\rho^*$	density contrast factor $(\rho_A - \rho_W)(\rho_M - \rho_A)/(\rho_M - \rho_W)$ (kg/m^3)
S(x, y)	influx or outflux of asthenosphere per unit area (m/s)
u_p(x, y)	plate velocity distribution (m/s)
u_0	reference plate velocity (m/s)
W	half width of symmetric ocean basin (m)
	Defined Variables
Rm	Ramberg number ($Rm = \frac{\Delta\rho^* g h_a^2}{\mu u_0}$)
d_{max}	maximum depth increase due to asthenospheric thinning (m)

leave the system with the subducting plates. The asthenospheric thickness is maintained at 225 km by a constant influx of new asthenosphere, uniformly distributed for all x, that balances the outflow of asthenosphere converted to lithosphere. The model has reflecting boundary conditions at the sides to simulate fixed zones of plate subduction. Grid spacing was decreased until little change in output was seen. Cases shown here have 100 km grid spacing.

[23] Figure 3a shows steady state asthenospheric thickness variations for two cases with different rates of plate divergence and no spreading center migration. Changing the spreading rate from 5 cm/a to 10 cm/a results in thinning of the subaxial asthenosphere by ~150 km. Figure 3b shows that changes in the rate of ridge migration have a smaller effect (~75 km) on the asthenosphere thickness under the spreading center.

[24] Our simple system of equations is nonlinear. Small changes in parameters can produce large changes in axial lithospheric thickness. Cases giving sizable variations in axial thickness with modest changes in spreading rate must be "close" to the point of zero asthenospheric thickness at the axis. By "close" we mean that a modest increase in spreading rate makes the axial lithospheric thickness go to zero. Running many 1-D numerical cases shows that quasi-steady state can be achieved on a short time compared to the age of oceanic plates. Asthenosphere thickens with distance from a spreading center and so causes shoaling of seafloor with increasing lithospheric age. However, the magnitude of the asthenospheric shoaling effect is a small fraction of seafloor deepening with age expected from lithospheric cooling and contraction.

[25] We did further 1-D model calculations to examine the effects of assumptions about the boundary between the asthenosphere and mesosphere (AM). First, we considered vertical motions of that boundary. In deriving equation (5) the mesosphere is taken to respond instantaneously to compensate pressure variations in the asthenosphere. The response of the mantle to vertical loads, such as those caused by changing ice sheets, is often treated in terms of flow of a viscous half-space. Pressure variations in the asthenosphere were treated as a vertical load on a viscous half-space and the response to those loads was computed at every model time step in the frequency domain. For a viscous half-space the time constant τ for exponential decay of a load is inversely related to the load wavelength, λ, as:

$$\tau = 4\pi\mu_m/\Delta\rho g\lambda \qquad (11)$$

where μ_m is the mesosphere viscosity, $\Delta\rho$ is the density contrast between the asthenosphere and the lithosphere, and λ is the load wavelength [e.g., *Turcotte and Schubert*, 2002]. An inverse Fourier Transform was used to return the deflections of the AM boundary to the spatial domain, where they were used in the next time step of the asthenospheric channel flow calculation.

[26] The time dependence in the model results from spreading center migration. For spreading center migration rates up to 5 cm/a and mesosphere viscosity up to 10^{21} Pa s we found no significant difference between these calculations and those using the assumption of instantaneous local isostasy of the AM boundary. The rate of ridge migration for the East Pacific Rise spreading center is about 2 cm/a [*Small*, 1998]. Thus, the assumption of local isostatic adjustment seems justified for he present problem.

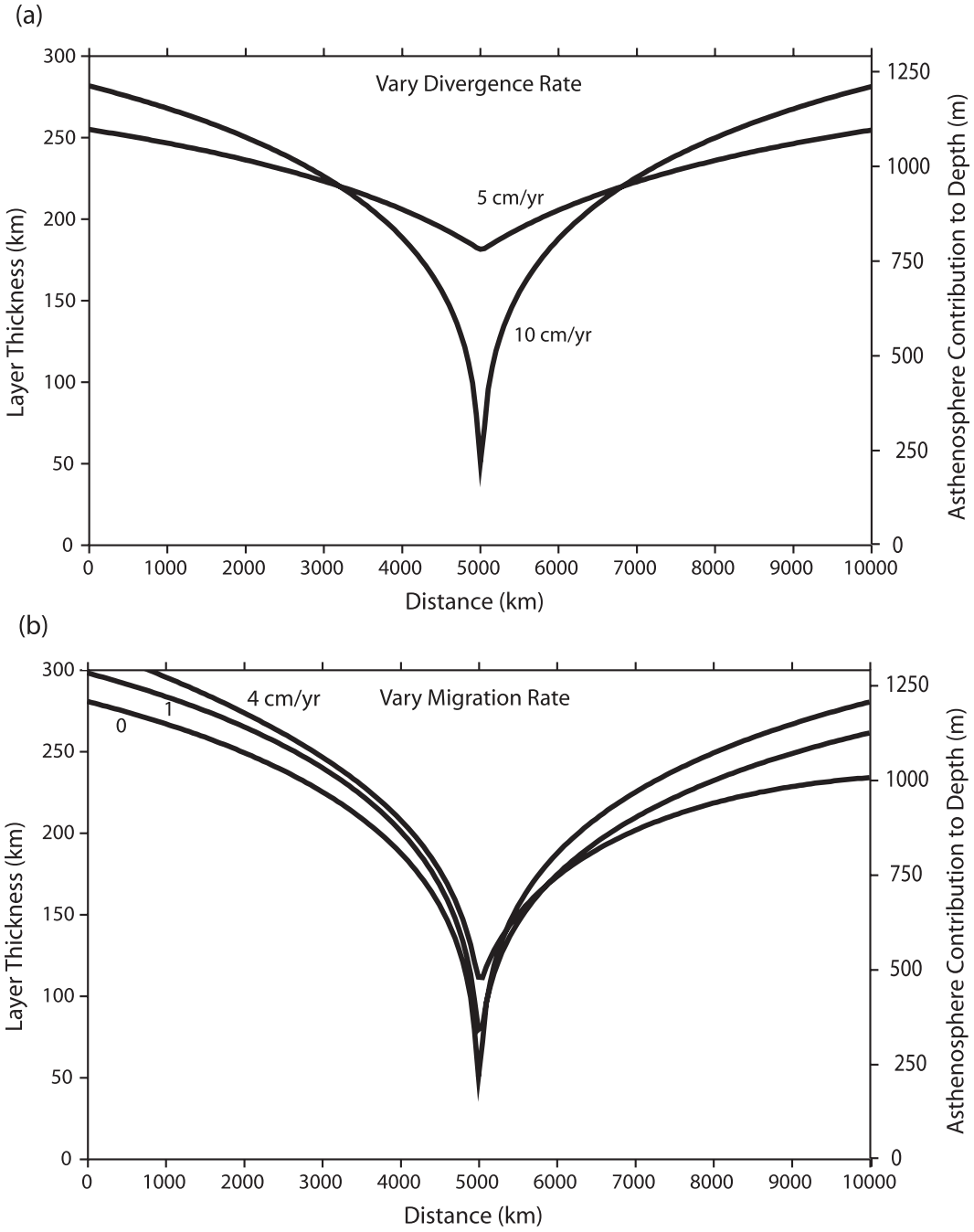

Figure 3. Illustrative results of one-dimensional thin layer calculations for asthenospheric flow driven by oceanic lithospheric plate divergence with spreading center migration from numerical solutions to one-dimensional versions of equations (7) and (8). Side boundaries are for no asthenospheric outflow, representing fixed subduction zones. Here the uniform influx of 1×10^{19} Pa s asthenosphere matches the removal of asthenosphere at the spreading axis to account for accretion of 100 km thick lithosphere. (a) Two cases with different divergence rates (= full spreading rate) and no migration of the spreading axis. (b) Illustration of how varying the migration rate has a small effect for cases with a divergence rate of 10 cm/a. For both cases the average asthenosphere thickness is 225 km.

[27] Second, we considered horizontal motion of the AM boundary. Equation (2) assumes no horizontal motion of that boundary. This may be justified if the motion of the mesosphere is slow compared to that of the asthenosphere, but some lateral motion of the boundary is likely. We considered the extreme condition of free slip of the base of the asthenosphere in a set of model calculations and found that by increasing the viscosity by a factor between 2 and 3 we got results

that were very similar to cases with a fixed asthenospheric base. This is easy to understand for the simplified cases described in Appendix A.

3.4. Critical Variables

[28] Numerical results show that varying the plate spreading velocity, and several other variables listed in Table 1, can affect the depth of the spreading axis. To get the magnitude of depth variation between the EPR and the PAZ for the measures spreading rate contrast requires that the faster spreading center must be close to a critical state where the axial asthenospheric thickness goes to zero. To gain insight into how parameters combine to allow that near-critical state we derived analytic solutions to the flow equation for some simple cases. As described in Appendix A, for flow driven only by plate drag (i.e., S = 0) and a symmetric spreading system as pictured in Figure 2, the asthenospheric thickness variations depend only on one parameter. When $Rm^{h_a}/_W = ({}^3/_2)^5 \sim 7$ the asthenospheric thickness at the axis goes to zero. For a larger value of this nondimensional quantity the axial layer has finite thickness. The magnitude of the depth anomaly caused by asthenospheric thickness variations depends on another parameter: $d_{\max}$. This variable must be of order 1000 m to explain the observed spreading center depth variations.

[29] These results indicate a fairly narrow range of reasonable model variables that are consistent with the observations. For example, consider a plate length L = 5000 km, a reference plate velocity u_0 = 10 cm/a, and ridge depth contrast 500 m. Then for $\Delta\rho^*$ = 10 kg/m^3 we predict that h_a should be in the range 250–300 km for a viscosity $\mu = 10^{19}$ Pa s. The asthenosphere could be as little as 100 km thick if the density contrast were $\Delta\rho$ = 20 kg/m^3, but the viscosity would have to be $\sim 10^{18}$ Pa s.

[30] Besides showing that our model depends mainly on two variables the analytic results make clear why previous "rigid base" models of asthenospheric flow failed to predict the observed magnitude of spreading center depth variations. Most previous treatments of asthenospheric flow assume that variations in the layer thickness are small compared to the average layer thickness [e.g., *Parmentier and Oliver*, 1979; *Chase*, 1979; *Yale and Phipps Morgan*, 1998]. This assumption greatly simplifies model calculations since the resulting equation for asthenospheric thickness, or dynamic topography, is linear.

[31] The analysis given in Appendix A shows that the linearized approach to solving equation (7) is valid for estimating the average variations in seafloor topography caused by plate motions, sources and sinks of asthenosphere. The average slope of seafloor depth and geoid were the main concerns of previous linearized model studies. In the present work we are concerned with how asthenospheric flow might affect the depths of the seafloor close to spreading centers. This is precisely where the nonlinear effects may be very significant, with the linearized approach underestimating spreading center depth anomalies by as much as 70%.

3.5. Comparison to the EPR

[32] The conceptual model of *Small and Danyushevsky* [2003] proposes that the difference in depth between the EPR and PAR could result from a difference in the rate of asthenospheric consumption between the two spreading centers. Asthenospheric consumption is considered the sum of sequestration into plates by cooling and advection away from the spreading center by viscous drag on the base of the plates. To show that this concept is consistent with not only the magnitude, but also the horizontal scale of spreading center depth variations we constructed 3-D numerical flow models including sources and sinks of asthensophere. They are 2-D thin channel models since only horizontal (x, y) variations in average layer velocities and thickness are computed. For simplicity we use a Cartesian geometry to represent a 10,000 km × 10,000 km region of plate driven asthenospheric flow, as shown in Figure 4. The velocity of the top of the asthenosphere is uniform over each of three plates. Model plate PAC is given a velocity representative of the Pacific plate of 9 cm/a to the west. The model plate ANT does not move, similar to the nearly stationary Antarctic plate, while the model plate NAZ moves east with a velocity of 6 cm/a, similar to the velocity of the Nazca plate. All sides are treated as reflecting boundaries. The east and west sides can be thought of as stationary subduction zones where asthenosphere is "trapped" by a "curtain" of subducting plate.

[33] The model spreading center where plate PAC diverges from the other two plates is a north–south line at 7,500 km from the west boundary of the model domain. The model EPR between plates PAC and NAZ has a divergence rate of 15 cm/a and migrates to the west at 1.5 cm/a. The model PAR spreads at 9 cm/a and migrates to the west at 4.5 cm/a. A number of model cases were tried with

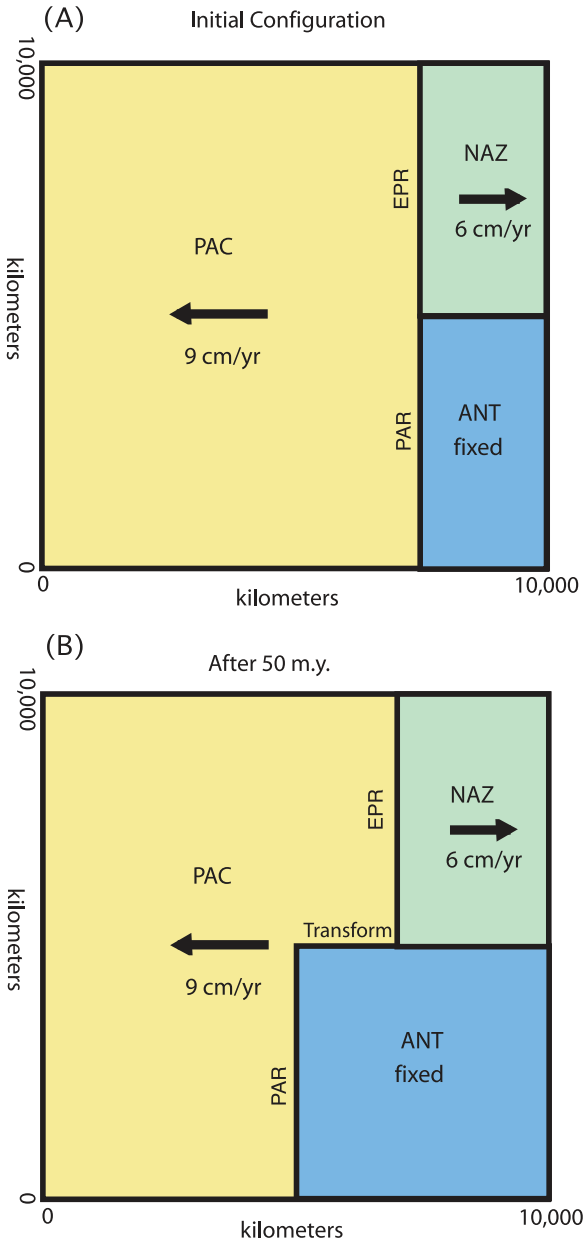

Figure 4. "EPR-PAR" model setup showing the effect of spreading center migration on plate boundary geometry. (a) Plan view of initial configuration of plates for very fast and fast sections of model spreading centers and 2-D thin layer asthenospheric flow. (b) Final configuration after 50 Ma of model time.

different values of the variable listed in Table 1, but we illustrate only one case "EPR-PAR1" here. We ran the model for 50 Ma as shown in Figure 4b. The other model parameters are: density contrast $\Delta\rho$ = 10 kg/m^3; average asthenosphere thickness h_a = 300 km, and; viscosity $\mu = 1.3 \times 10^{19}$ Pa s. All transfer of asthenosphere into 100 km thick model lithosphere occurs close to the spreading centers and the uniformly distributed asthenospheric influx is enough to keep the average asthenospheric thickness constant. Cases with 50 and 100 km grid spacing were run with no significant differences in results.

[34] As in the 1-D thin layer models the asthenosphere thins under the spreading centers and thickens toward the model subduction zones. The thickness is nearly constant under the stationary ANT plate. Figure 5 shows the depth variations caused by asthenospheric thickness variations at the end of the model run. Figure 1b shows model depth variations for lines along the axes of the spreading centers. Note that the model EPR is about 400 m deeper than the model PAR and that the asthenosphere beneath both ridges is fairly uniform in thickness in agreement with depth observations [*Small and Danyushevsky*, 2003]. The combined effects of lithospheric cooling and asthenospheric thickness variations are shown in Figure 5b. The lithospheric cooling was included by using a simple half-space cooling model producing subsidence of 300 m per (Ma)$^{1/2}$ [e.g., *Parsons and Sclater*, 1977; *Stein and Stein*, 1992] and this shows that the lithospheric cooling effect dominates that due to asthenospheric variations away from the spreading axis.

4. Australian-Antarctic Discordance

[35] The greatest depths along any spreading center occur south of Australia in a region known as the Australian-Antarctic Discordance [*Weissel and Hayes*, 1974] or AAD (see Figure 6). The ~1000-km-long AAD is not only nearly a kilometer deeper than normal spreading centers, but the ridge flanks are extremely rugged and cut by a series of closely spaced fracture zones [*Weissel and Hayes*, 1974; *Vogt et al.*, 1983; *Marks et al.*, 1990, 1991; *Christie et al.*, 1998]. The average depth within 50 km of the spreading center (Figure 9b) shows a gradual decrease over a few thousand kilometers from the AAD. In contrast to the smooth variation in bathymetry, the isotopic character of the mid-ocean ridge basalts changes more abruptly at the AAD. To the west the rocks show clear Indian Ocean isotopic content while to the east the rocks are isotopically like those found along spreading centers in the Pacific [e.g., *Klein et al.*, 1988; *Christie et al.*, 2004].

[36] The crust in the AAD is about half as thick as normal oceanic crust [*Tolstoy et al.*, 1995] indicating reduced melting below this ridge. Major element

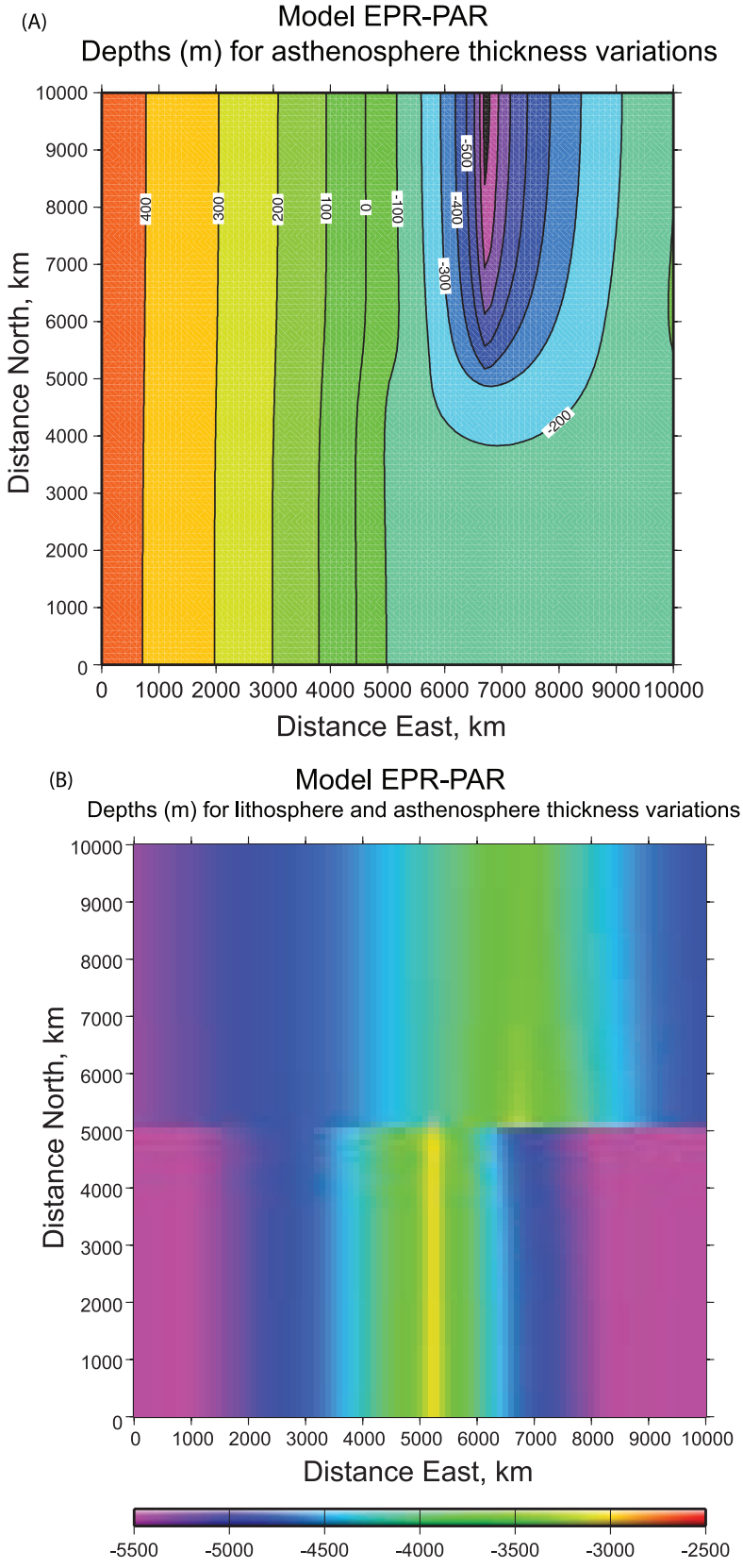

Figure 5. Results of 2-D "EPR-PAR1" model in plan view showing (a) the depth variations in meters produced by asthenospheric thickness variations and (b) combined depth variations due to both asthenospheric and model lithospheric thickness variations. Note that axial depths from this model shown in Figure 1b.

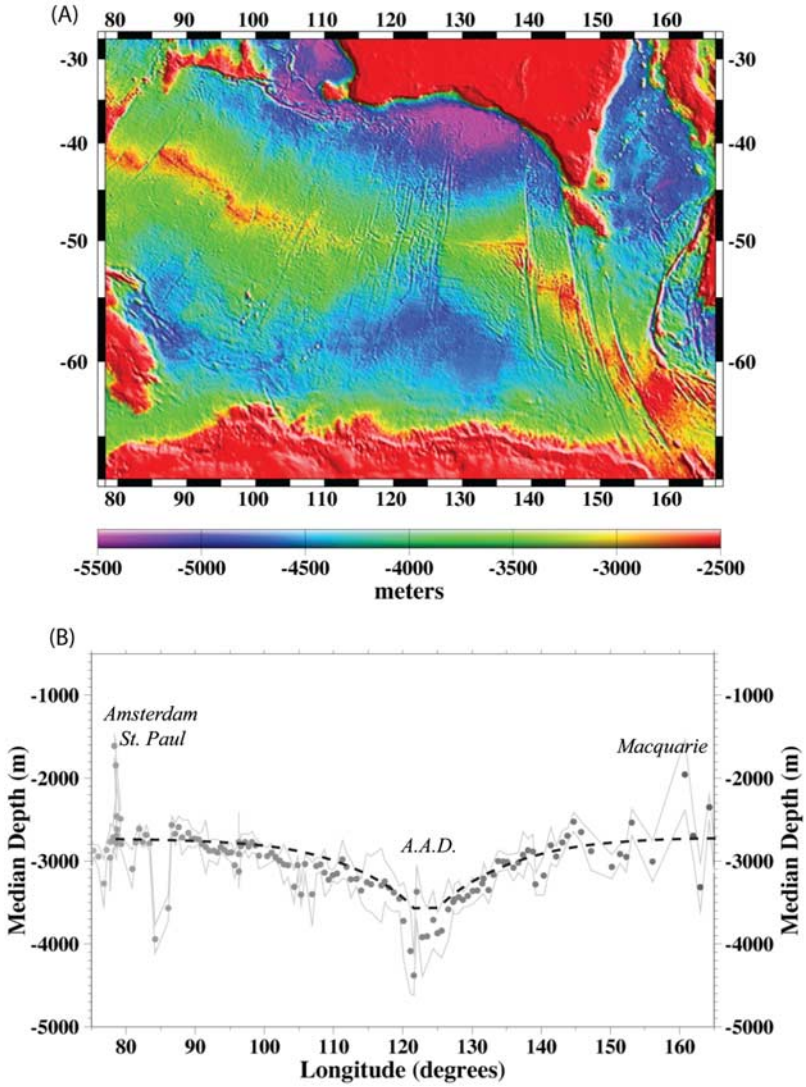

Figure 6. (a) Shaded relief bathymetry of the region between Australia and Antarctica. Note the fairly normal ridge depth along the Southeast Indian Ridge gradually deepening toward the Australian-Antarctic Discordance that is cut by many closely spaced fracture zones. (b) Average depth within 50 km of the ridge axis along the ridge segments surrounding the AAD. Dashed line shows predicted axial depth variations for model experiments described in section 4.2.

geochemistry is consistent with reduced temperatures in the mantle beneath the discordance [e.g., *Klein and Langmuir*, 1987], but it is also possible the low melt production results from thinner-than-normal asthenosphere below the discordance.

[37] Most of the ocean basin between Australia and Antarctica is younger than 40 Ma [*Marks et al.*, 1999]. Australia and Antarctica were linked until Australia began to rift away in the mid-Cretaceous [*Veevers*, 1986]. The rate of rifting and seafloor spreading was as slow as 1 cm/a until about 40 Ma when the spreading rate jumped to ~6 cm/a [*Marks et al.*, 1999; *Müller et al.*, 2000].

[38] The AAD is generally viewed as an area of mantle downwelling, or reduced upwelling, somehow related to lateral temperature variations in the mantle [*Klein et al.*, 1988; *Alvarez*, 1990; *West et al.*, 1994, 1997; *Lin et al.*, 2002; *Cochran et al.*, 1997; *Baran et al.*, 2005]. *Gurnis et al.* [1998] use plate reconstructions to show that cold, dense slabs of previously subducted lithosphere should exist at ~1000 km depth below the AAD. They then use mantle flow models to suggest the possibility that these negatively buoyant loads could pull down the surface of the Earth in a pattern similar to that of the AAD. More recent variants on this idea include a cold wedge of highly depleted mantle that over-

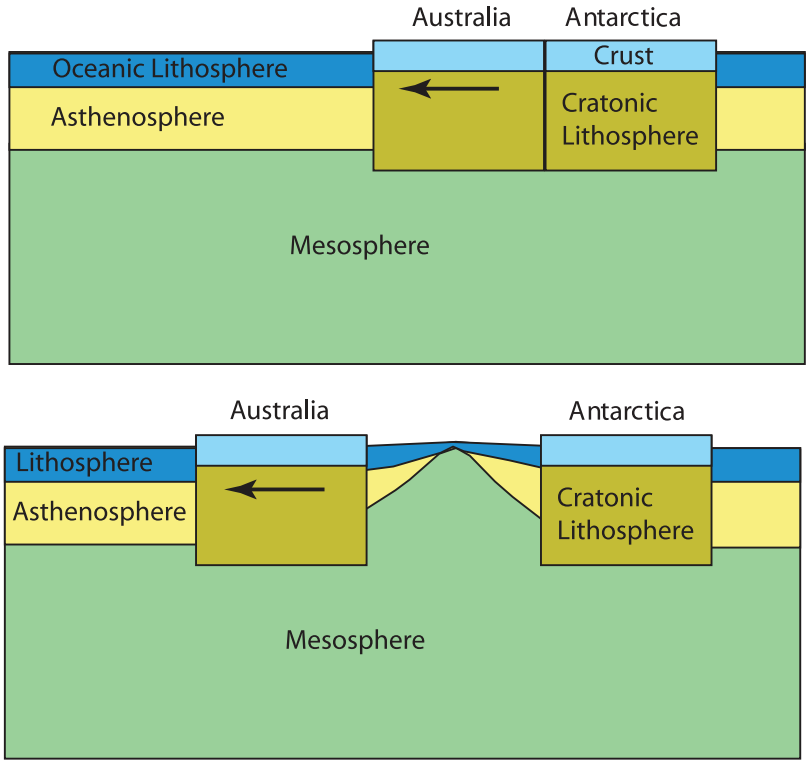

Figure 7. Model cross section showing the geometry of continental blocks with lithospheric roots thicker than the asthenospheric layer. The spreading center separating those blocks may be starved of asthenosphere since the thick blocks do not allow asthenosphere to pour in as easily as it would without the blocks.

lies the subducted slabs [*Gurnis and Müller*, 2003]. These models must assume that the mantle viscosity in this region does not increase appreciably with depth.

[39] A uniform viscosity mantle, required by *Gurnis et al.* [1998] and [*Gurnis and Müller*, 2003], is hard to reconcile with a variety of geophysical observations. For example, the lack of a great topographic depression over presently subducting slabs combined with a large geoid high is often used as evidence of a strong increase in viscosity with depth [e.g., *Richards and Hager*, 1984; *Davies*, 1999]. Postglacial rebound studies [e.g., *Lambeck et al.*, 1998] and studies of relations between seismic velocity anomalies and geoid anomalies [e.g., *King and Masters*, 1992] are also consistent with viscosity increasing with depth. Laboratory studies on olivine, the dominant mantle mineral, suggest that viscosity should increase with pressure and therefore depth [e.g., *Kirby*, 1983]. Since slab induced downwelling model for the AAD requires little or no increase in viscosity with depth it is worth considering an alternative.

4.1. Separation of Continental Roots

[40] Here we examine whether flow of shallow low-density asthenosphere may offer an explanation of the anomalies associated with the AAD, including its great depth, thin crust and isotopic pattern. The basic idea is that asthenospheric flow toward a spreading center could be restricted by the separation of blocks of thick continental lithosphere (Figure 7). Seismic measurements indicate that the lithosphere beneath old continental cratons can be several hundred kilometers thick [e.g., *Jordan*, 1981]. Australia and East Antarctica are largely cratonic and show high seismic velocities indicative of lithosphere down to several hundred kilometers [*Simons et al.*, 1999; *Ritzwoller et al.*, 2001].

[41] Figure 7 is an idealized cross section showing how motion of thick lithospheric blocks might affect asthenospheric thickness below an adjacent spreading center. As blocks of thick continental lithosphere move apart asthenosphere will pour in to the gap beneath the new ocean basin. For a reasonable rate of supply from below, the new basin must have inflow from its sides if astheno-

sphere is to fill in below the widening basin and feed the spreading center "sink." The question for us is whether asthenosphere flowing in from the side can supply all that asthenosphere, or whether the asthenosphere might "run out" or be thinned to zero thickness below a portion of the spreading center. This would leave a section of spreading center that is deeper both because of the lack of buoyant asthenosphere and because of the reduction in crustal thickness due to upwelling and melting of cooler mesosphere there.

[42] The amount of asthenosphere converted to lithosphere along a spreading center of length L_C equals about $u_p h_a L_C/2$ where is the lithosphere thickness and u_p is the plate divergence rate. Assume that the asthenosphere is zero thickness at the center of the ocean basin of length L_c. If the layer thickness is h_a at the edge of the basin then the pressure gradient driving flow into the nascent basin is $2\Delta\rho^* g\ h_a/L_c$. Multiplying this gradient by $Wh_a^3/12\mu$, where W is the half-width of the nascent basin, give the pressure driven flux coming into the sides of the ocean basin. These fluxes can be equal given:

$$Rm\frac{h_a}{W} \approx 6\left(\frac{L_C}{W}\right)^2 \tag{12}$$

If $Rm(h_a/W)$ is of order 10, as required in the Pacific type models, this condition would be met for an ocean basin that is about as wide as the deep-rooted continent is long. For a narrower basin we expect significant thinning of the asthenosphere along the spreading center between the separating continents. The distance between Australia and Antarctica (i.e., W) is indeed close to the length of the conjugate continents (i.e., L_c). The numerical models described below are designed to see if this rough calculation is correct.

4.2. Comparison to the AAD

[43] To test the viability of this concept requires numerical consideration of flow around lithospheric blocks. Thus, we modified the 2-D thin channel numerical models described above to include blocks of lithosphere so thick as to act as barriers to asthenospheric flow. For simplicity we assume that the continental lithosphere is thicker than the maximum thickness of the asthenosphere so it can only flow around but not under the blocks (Figure 7). We also neglect the delivery of asthenosphere to the base of the continental lithosphere to avoid the complication related to subcontinental asthenospheric flow. Two continental blocks are set up with a width of 3000 km in the east–west direction and 2000 km in the north–south direction.

[44] The velocity of the top of the asthenosphere is uniform over each of two plates surrounding the two continental blocks. Rather than simulate the complex history of opening of very slow then fast separation of Australia from Antarctica we focus on the period of faster spreading of the last 40 Ma. The blocks are initially set 800 km apart with a linear, east west trending spreading center midway between them as shown in Figure 8. The initial separation represents the opening of the continents during the early, slow phase of continental extension. At the start of the model calculation the asthenosphere has a uniform thickness of 300 km everywhere except under the model continental blocks. Model plate AUS is given a velocity of 6 cm/a to the north, representative of the absolute motion of the Australian plate for the last 40 Ma. The model plate ANT does not move, similar to the nearly stationary Antarctic plate. The southern, eastern and western sides are treated as reflecting boundaries. The northern side is an advective outflow where the asthenosphere flux out equals the asthenospheric thickness times the rate of plate motion. It is hard to know the most reasonable boundary conditions to use in the tectonically complex region north of Australia. The boundary condition approximates northward migration of a subduction zone. We ran the model for 40 Ma of model time to produce the final plate configuration shown in Figures 8b and 9.

[45] A case "AAD1" was run with the same asthenospheric properties of density and viscosity as for the "EPR-PAR1" model run described earlier. The density contrast with the mesosphere was 10 kg/m^3 and the viscosity was 1.3×10^{19} Pa s. As with the earlier case, the initial thickness of the asthenosphere was set to 300 km and all transfer of asthenosphere into 100 km thick model lithosphere occurs at the spreading centers. The uniformly distributed asthenospheric influx is enough to keep the average asthenospheric thickness constant with the same boundary conditions as for the EPR-PAR models. However, the northern boundary condition of advective outflow leads to a progressive reduction of the average asthenosphere thickness by about 20% over the course of a model calculation.

[46] The calculation shows that separation of deep-rooted blocks changes the pattern of asthenospheric flow toward the spreading center where asthenosphere is "consumed" to make new lithosphere.

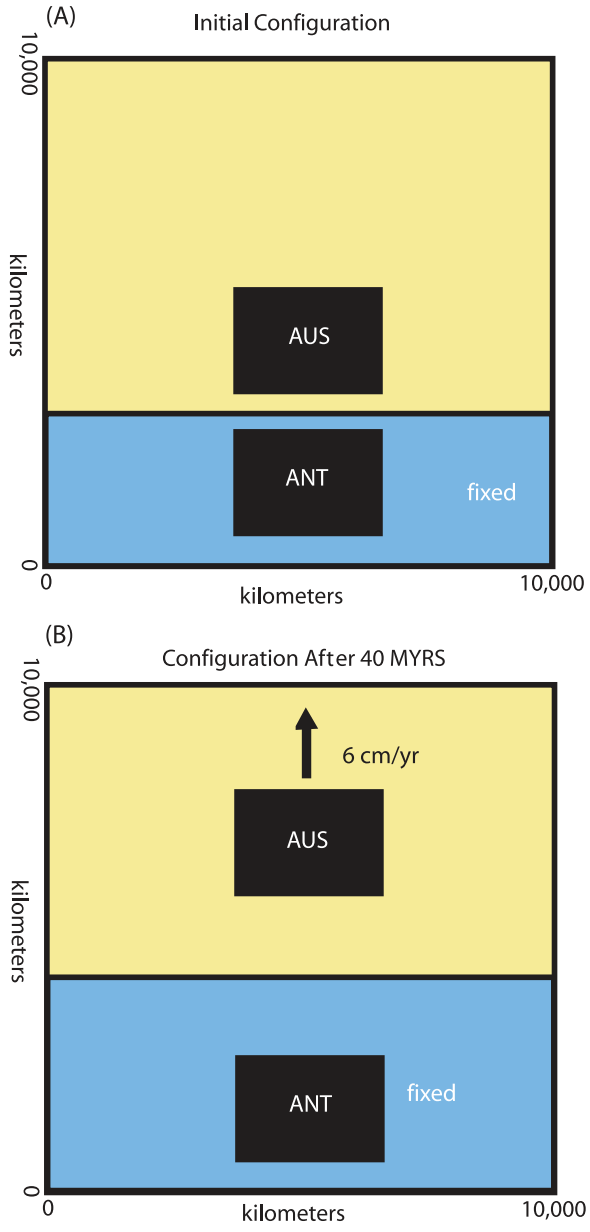

Figure 8. AAD model setup showing two continental lithospheric blocks separated by a 6 cm/a spreading center showing (a) plan view of initial configuration of plates and (b) final configuration after 40 Ma of model time.

The widening of the initially narrow ocean basin also reduces the average asthenosphere thickness between the separating continents. After only a few hundred kilometers of spreading the asthenosphere near the axis between the blocks is exhausted so the asthenospheric thickness there is zero. The asthenosphere can flow laterally from the two sides and the inflow can keep up with the loss of asthenosphere at the axis. This basic pattern is maintained through the 40 Ma of the model calculation. Figure 9a shows the final distribution of depth variations caused by variations in the asthenospheric thickness. Note the smooth variations in the depth anomaly over several thousand kilometers of spreading center either side of the region of greatest depths. The combined effects of litho-

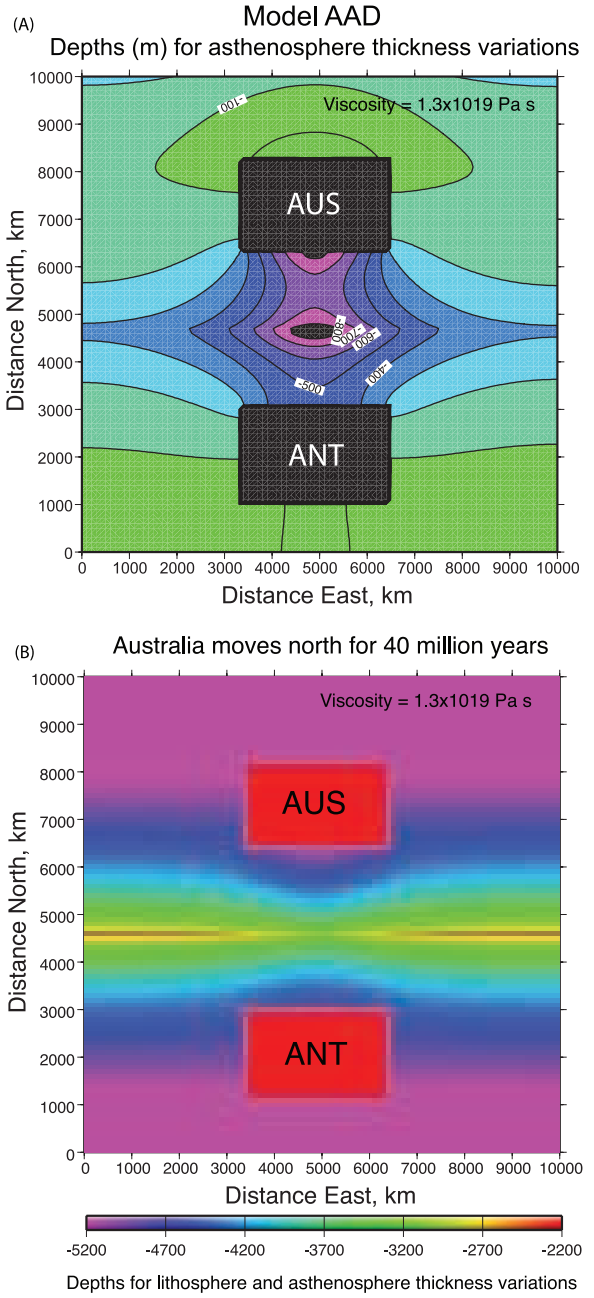

Figure 9. Plan view of 2-D "AAD1" model results showing (a) the depth variations in meters produced by asthenospheric thickness variations and (b) combined depth variations due to both asthenospheric and model lithospheric thickness variations. Note that axial depths from this model are shown in Figure 6b.

spheric cooling and asthenospheric thickness variations are shown in Figure 9b. As before the lithospheric cooling was included by using a simple half-space cooling model with subsidence of 300 m per square root of millions of years.

[47] The wavelength of model depth variations shown in Figure 9 is quite similar to the observed variations and the depth profile for the end of the model run is shown on Figure 6. The amplitude of the depth variations slightly is less that that observed and this may be because we did not include variations in crustal thickness likely to occur in the model where the asthenosphere is exhausted. There the cooler mesosphere would melt much less than hotter asthenosphere producing thinner crust. Three kilometers of crustal thickness reduction should add ~400 m depth assuming a crustal density of 3000 kg/m^3 compared to a mantle density of 3300 kg/m^3. This would make the model deep axial zone about 1300 m deeper than the spreading centers far away and this is comparable to the observed deepening.

5. Discussion

[48] It is surprising how well this simple model mimics the spatial distribution of spreading center and off-axis depths for the Pacific and the AAD regions, since many potentially important factors were not considered. The essential feature of this model is that the asthenosphere is lower in density than the underlying mantle. The 100°C temperature contrast between the asthenosphere and mesosphere is within the range of temperature variation along plume-affected ridges [e.g., *Schilling*, 1991]. The assumed viscosity of the asthenosphere is also not unreasonable in terms of other estimates of shallow mantle viscosity [e.g., *King*, 1995]. Interestingly, the viscosity is low enough, given a layer thickness over a hundred kilometers, so that the viscous drag on a large, fast plate is smaller than the estimated ridge push force [e.g., *Turcotte and Schubert*, 2002]. Implications of buoyant asthenosphere flow for plate-scale forces and the migration of subduction zones is discussed by *Nagel et al.* [2008].

[49] The model reproduces observed depth trends even if the mesosphere is not stationary, but is dragged along by the flow of the asthenosphere. In contrast, temporal and spatial variation in the supply of asthenosphere would significantly affect the model results, but these are not required. The history of plate motions on a sphere, the proximity of subduction zones and more complex mantle rheologies should be considered in future models. However, it appears that that plate divergence rate and motion of thick lithosphere have observable effects on the depth of ridges.

[50] The major place where the model results differ from observations along the EPR is close to the Easter Hot spot where extra hot asthenosphere may be injected by a major plume. Also, the simple models for continental lithospheric separation do not produce the magnitude of depth variations seen along and adjacent to the AAD. This is to be expected since we did not account for the reduced mantle melting that might result in thinner crust in the AAD.

[51] Seismic evidence from the Pacific does not clearly support or refute this model. Seismic anisotropy in the shallow oceanic mantle is dominated by plate driven shear deformation, particularly in the Pacific [e.g., *Becker et al.*, 2003]. This is consistent with our model, however plate motion would still shear the mantle even without hot, buoyant asthenosphere. *Nettles and Dziewoński* [2008] have recently estimated that the region of strong seismic anisotropy under the pacific plate is largely confined to the 100–200 km depth range. This is consistent with strain concentrating in a low-viscosity shallow asthenosphere. Our model should result in greater upwelling and melting on the west side of the EPR and this is consistent with the seismically observed asymmetry in the low-velocity region below the southern EPR [*Forsyth et al.*, 1998].

[52] On the scale of the Pacific Plate there is no clear seismically observed thickening of a low-velocity zone with distance from the spreading center [e.g., *Nishimura and Forsyth*, 1985], as might be expected for this model. Two things may explain this apparent inconsistency. First, the magnitude of the expected velocity decrease due to high asthenospheric temperatures is small compared to the velocity increase due to lithospheric cooling. Thus, the signal would be masked by the lithospheric cooling velocity increase. Second, there should be no sharp base of the asthenosphere. The cooler part of the asthenosphere is dense and so could sink to the base of the layer where temperatures should grade into the underlying mesosphere. If the gradation occurs over 100 km then the negative temperature gradient would be as little as 1°C/km. This is less than the adiabatic

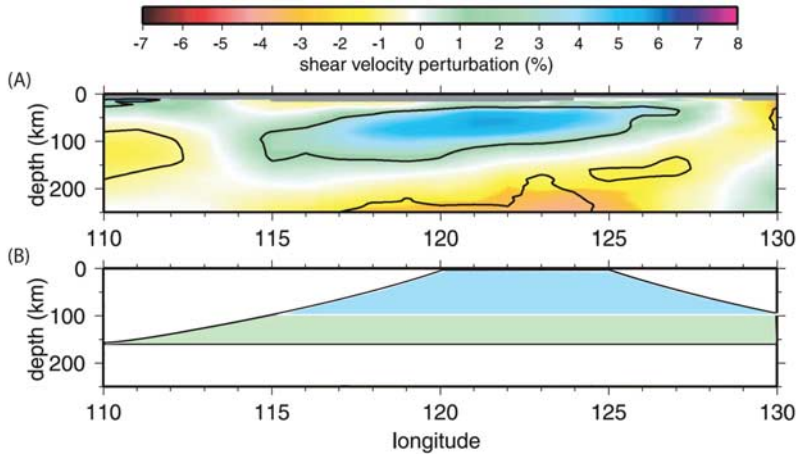

Figure 10. (a) Seismic shear wave velocity anomalies estimated for the upper mantle near the AAD from *Ritzwoller et al.* [2003]. The cross section shown is along latitude 50°S. (b) Pattern of seismic velocity anomalies along the model spreading for case AAD1. This assumes that temperature differences relative to the model temperature at 2000 km from the center of the model AAD spreading center produces a 1% increase in shear wave velocity for a 100°C temperature drop. For depths less than 100 km the 100°C cooler temperatures are assumed to increase shear velocities by 4% because of reduced melting. The very high-velocity anomalies caused by crustal thinning are indicated at the top of the model cross section.

gradient and seismic detection of this small gradation might be extremely difficult.

[53] Analysis of seismic data covering the region south of Australia by *Ritzwoller et al.* [2003] indicate higher than normal seismic velocities in mantle shallower than ~120 km depth under the AAD (Figure 10a). *Ritzwoller et al.* [2003] note that the lateral resolution of the seismic velocity estimates are not as good as the vertical resolution, but that their measurements are consistent with temperatures 100–200°C cooler less than 120 km below the AAD relative to more normal ridge segments. It is difficult to understand how a deep mantle density anomaly suggested by *Gurnis et al.* [1998] could produce this shallow seismic velocity anomaly, but *Ritzwoller et al.* [2003] see this as the only explanation for their observations. *Christie et al.* [2004] detail observations that are difficult to reconcile with entrainment of a residual cold arc mantle as suggested by *Gurnis et al.* [1998] and *Gurnis and Müller* [2003]. They note that the NW–SE trend of the high-velocity anomaly in the shallow mantle adjacent to the AAD seen by *Ritzwoller et al.* [2003] is not consistent with the predicted pattern of N–S Pacific paleosubduction zone inferred by *Gurnis et al.* [1998]. Three-dimensional flow model calculations by *Lin et al.* [2002] specifically investigate what conditions would allow upwelling and entrainment of cold mantle beneath the AAD. For realistic viscosity structures they found that upwelling of cool material is likely only at the initiation of separation of deep, strong continental lithospheric roots. This is hard to reconcile with the persistence of the AAD to the present day.

[54] The shallow depth range (<120 km) of the mantle anomaly imaged by *Ritzwoller et al.* [2003] and earlier by *Forsyth et al.* [1987] are precisely what the present model predicts. If temperature controlled melting has a strong affect on the seismic velocities then model AAD1 could give a good fit to the seismic model since the cold mesosphere pulled up under the AAD in our model would not melt until a much shallower depth than along adjacent segments (see Figure 10b). Normal asthenosphere may begin to melt at 100–120 km depth [e.g., *Klein and Langmuir*, 1987] while colder mesosphere might not melt until it reached a much shallower depth. The shallower onset of melting beneath the AAD would lead to higher velocities there. This interpretation is consistent with the thinner oceanic crust in the AAD inferred from seismic refraction measurements recently analyzed by *Holmes et al.* [2008] and R. C. Holmes (personal communication, 2009). Our asthenosphere flow model could produce a shallower depth range of seismic anomalies were we to adjust the model parameters to allow a thinner average asthenospheric layer. To fit the depth data, this would require an increase the temperature contrast (and so the density contrast) between the astheno-

sphere and mesosphere and a decrease the asthenospheric viscosity.

[55] The sharp boundary in isotopes seen at the AAD [e.g., *Christie et al.*, 2004] may be due the fact that the asthenosphere of the Pacific and that of the Indian Ocean have long been separated. One can speculate that different deep mantle source regions imparted the different isotopic signature to the asthenosphere of the Pacific compared to that of the Indian Ocean. Asthenosphere moving at greater than plate velocities could become well mixed given sufficient time. The residence time for asthenospheric material beneath a large ocean basin should be ~500 Ma, long enough for considerable homogenization. In our model for the AAD there is no mixing of the Pacific and Indian Ocean asthenosphere along the spreading boundary since the asthenosphere thickness there goes to zero.

[56] The key requirement of our model is that the shallow mantle be less dense than the underlying mantle. The low density is most easily explained if the asthenosphere is supplied by hot, buoyant mantle plumes as suggested by *Morgan* [1971, 1972a, 1972b]. Plumes have come to be thought of as the hot, enriched upwellings that melt to produce ocean island basalts (OIBs). This creates a problem for the plume-fed asthensophere hypothesis that relates to the flux of heat carried by OIB plumes. Only about 10% of heat carried out of the Earth's interior is delivered by such plumes, on the basis of the depth anomalies around hot spots [e.g., *Sleep*, 1990]. The bulk of Earth's heat escapes as asthenosphere is cooled to make oceanic lithosphere.

[57] We conjecture that most of the hot asthenosphere that supplies the growing lithospheric plates is delivered from the deeper mantle by depleted mantle plumes. Depleted mantle plumes do not have to be as hot as OIB plumes to be buoyant. The enrichment of iron and aluminous phases in OIB source plumes makes them denser than depleted mantle [e.g., *Oxburgh and Parmentier*, 1977]. Thus, OIB plumes must be hot by an extra ~100°C to overcome the compositional effect and make them positively buoyant. Depleted plumes can be buoyant for a much lower temperature contrast with the surrounding mantle.

6. Summary

[58] Variations in spreading center depth are best explained by plate-driven flow of low-density asthenosphere. The greater depth of the East Pacific Rise can be explained by its very fast spreading rate relative to its comparatively slow migration rate according to this model. The very deep Australian-Antarctic Discordance is deep because it is the fastest opening small ocean basin and the motion of adjacent thick continental lithosphere disrupts the flow of asthenosphere into that region. The model also accounts for the contrast in isotopes observed across the AAD and the reduced crustal thickness there. To our knowledge, kinematically modulated plate driven asthenospheric flow is the only proposed quantitative explanation for the anomalous depth of the EPR. The fact that the same asthenospheric properties of thickness, viscosity and density can fit the characteristics of both regions lends credence to this model. We speculate that hot, buoyant asthenosphere may be supplied from the deeper mantle mainly by upwelling depleted plumes as opposed to OIB plumes.

Appendix A: Analytic Treatment of Thin Viscous Layer Flow Cases

[59] We can gain some insight into the how parameters affect asthenospheric thickness, and the related model seafloor depth, by considering analytic solutions for simple cases of thin-layer viscous asthenospheric flow. This also allows illustration of the difference between solutions to the nonlinear, thin viscous layer equation (equation (8)) and solutions of the linearized version of that equation used in most previous models of asthenospheric flow [e.g., *Chase*, 1979; *Parmentier and Oliver*, 1979; *Yale and Phipps Morgan*, 1998].

[60] Asthenospheric flow can be driven by a combination of plate motion that drags the asthensosphere with the plate and by addition of fresh asthensophere in one area and withdrawal in another (here termed sources and sinks). Analytic solutions to equation (8) can be derived if we consider just one of those driving factors at a time.

A1. Plate Driven Flow

[61] The simplest case to consider is for asthenospheric flow driven only by plate motions with no sources or sinks. Consider the case shown in Figure 2, but for negligible thickness, but rigid plates. Assume that the left edge of the asthenospheric layer (the subduction boundary) is at $x = 0$ and the center of the region (the spreading center is at $x = W$. The plate velocity $u_p = -u_0$ for $0 < x < W$ and $u_p = +u_0$ for $W < x < 2W$. For steady state

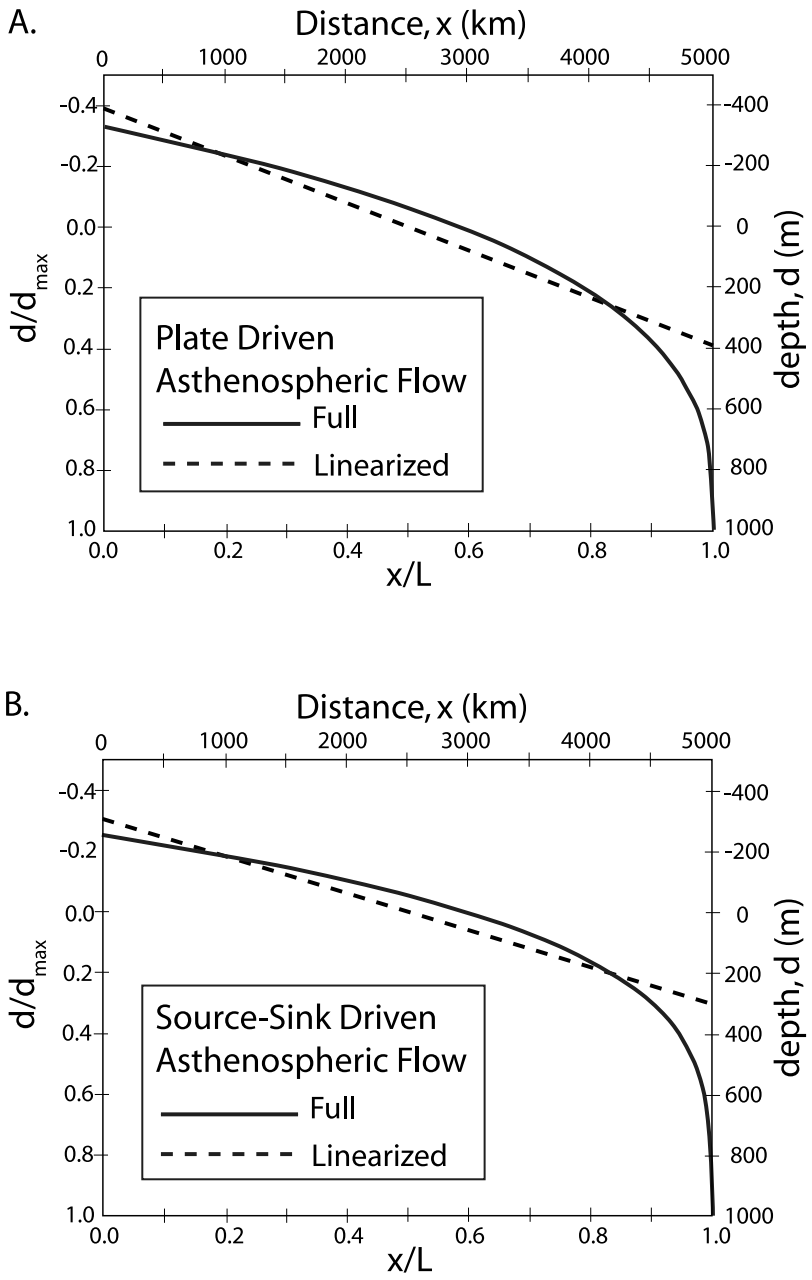

Figure A1. Results of analytic predictions of asthenospheric thickness versus distance for two simplified cases for half of a symmetric model ocean basin as shown in Figure 2. Also shown on the axis at the right is the contribution of the asthenospheric thickness variations to ocean depth. Solid lines show the solutions of the full thin viscous layer equation for asthenospheric flow, while the dashed lines show the solution of the linearized version of that equation. Each nonlinear case is for the critical condition that gives zero asthenospheric thickness at the spreading axis ($x = W$), and the linearized case is for the same parameters. The top axis is for $W = 5000$ km, and the right axis is for $d_{max} = 1000$ m. (a) The analytic results for flow driven only by plate drag as described by equations (A2) and (8). The linearized predicted axial depth given by equation (A5) is 60% less than for the nonlinear solution. (b) The case of flow driven only by an asthenospheric sink at $x = W$ and a single source at $x = 0$ as given by equation (A7). The linearized predicted effect on axial depth is 70% less than for the nonlinear solution.

conditions and no variation in the y direction equation (7) becomes:

$$\frac{\Delta\rho^* g h^2}{6\mu}\frac{\partial h}{\partial x} = u_p \tag{A1}$$

We can consider only the region between $x = 0$ and $x = W$ since symmetry demands that there be no flux at those positions. As long as the asthenospheric layer thickness is not zero between $x = 0$ and $x = W$ the thickness variation can be expressed as:

$$h(x) = h(0)(1 - C_0 x)^{1/3}$$

where

$$C_o = \left(\frac{h_a}{h(0)}\right)^2 \frac{18}{h(0)Rm}. \tag{A2}$$

A closed form solution can be obtained when the layer thickness at the spreading axis goes to zero (i.e., $h(W) = 0$). That occurs when $C_0 = 1/W$ which requires that $h(0) = (4/3)h_a$ and that the Ramberg number equals the critical value:

$$Rm_{cr} = \left(\frac{3}{2}\right)^5 \frac{W}{h_a}. \tag{A3}$$

Figure A1a shows both the asthenospheric thickness variations given by the analytic solution of equation (A1) and the associated ocean depth variations calculated using equation (8) for the critical value of the Ramberg number.

[62] The solution to the linearized version of equation (A1) gives:

$$\frac{\partial h}{\partial x} = \frac{6}{Rm}. \tag{A4}$$

Using equation (8) the variation in seafloor depth resulting from such asthenospheric thickness variations can be described as:

$$\frac{\partial d}{\partial x} = \frac{(\rho_M - \rho_A)}{(\rho_M - \rho_W)}\frac{6}{Rm} = \frac{6u_0\mu}{(\rho_A - \rho_W)gh_a^2}. \tag{A5}$$

Note that for the linearized solution the seafloor depth variation does not depend on the density of the mantle underlying the asthenosphere. The dashed line on Figure A1a shows the linear solution for the same parameters as for the nonlinear case that has zero layer thickness at the axis. The linearized solution is close to the full solution everywhere except close to the spreading axis. At the spreading center the linear solution predicts a 39.5% reduction in layer thickness while, of course, the full solution gives a 100% reduction.

A2. Source-Sink Driven Flow

[63] A similar analysis can be done for the simplified case of flow driven only by one source and one sink of asthenosphere and no plate driven flow. As with the previous example, we do not consider it to be realistic and we only do this to elucidate the behavior of the system. If the sources and sinks are applied as line sources that are uniform in the y direction and are applied at $x = 0$ and $x = W$ then equation (7) becomes:

$$\frac{\partial}{\partial x}\left(\frac{\Delta\rho^* g h^3}{12\mu}\frac{\partial h}{\partial x}\right) = 0. \tag{A6}$$

For a line sink ($=-q_s$) at the spreading center ($x = W$) and a line source ($=q_s$) at the site of plate downwelling ($x = 0$) the layer thickness can be expressed as:

$$h(x) = h(0)(1 - C_1 x)^{1/4}$$

where

$$C_1 = \frac{48\mu q_s}{\Delta\rho^* g h^4(0)}. \tag{A7}$$

[64] Figure A1b shows the depth variations related to variations in thickness of the asthenosphere layer when $h(W) = 0$, which occurs when $C_1 = 1/W$ which requires that $h(0) = (5/4)h_a$. The corresponding linearized solution is also shown and it gives just under 30% of the ridge axis depth anomaly given by the nonlinear treatment.

Acknowledgments

[65] Thanks to David Christie, W. Chadwick Holmes, and Peter van Keken for helpful comments.

References

Albers, M., and U. Christensen (2001), Channeling of plume flow beneath mid-ocean ridges, *Earth Planet. Sci. Lett.*, *187*, 207–220, doi:10.1016/S0012-821X(01)00276-X.

Alvarez, W. (1990), Geologic evidence for the plate driving mechanism: The continental undertow hypothesis and the Australian-Antarctic Discordance, *Tectonics*, *9*, 1213–1220, doi:10.1029/TC009i005p01213.

Baran, J. M., J. R. Cochran, S. M. Carbotte, and M. R. Nedimovic (2005), Variations in upper crustal structure due to variable mantle temperature along the Southeast Indian

Ridge, *Geochem. Geophys. Geosyst.*, *6*, Q11002, doi:10.1029/2005GC000943.
Batchelor, G. K. (1967), *An Introduction to Fluid Dynamics*, 635 pp., Cambridge Univ. Press, Cambridge, U. K.
Becker, T. W., J. B. Kellogg, G. Ekstrom, and R. J. O'Connell (2003), Comparison of azimuthal seismic anisotropy from surface waves and finite strain from global mantle-circulation models, *Geophys. J. Int.*, *155*, 696–714, doi:10.1046/j.1365-246X.2003.02085.x.
Bird, P. (1991), Lateral extrusion of lower crust from under high topography in the isostatic limit, *J. Geophys. Res.*, *96*, 10,275–10,286, doi:10.1029/91JB00370.
Buck, W. R. (1991), Modes of continental lithospheric extension, *J. Geophys. Res.*, *96*, 20,161–20,178, doi:10.1029/91JB01485.
Buck, W. R. (1992), Global decoupling of crust and mantle: Implications for topography, geoid and mantle viscosity on Venus, *Geophys. Res. Lett.*, *19*, 2111–2114, doi:10.1029/92GL02462.
Buck, W. R., and E. M. Parmentier (1986), Convection beneath young oceanic lithosphere: Implications for thermal structure and gravity, *J. Geophys. Res.*, *91*, 1961–1974, doi:10.1029/JB091iB02p01961.
Buck, W. R., C. Small, W. B. F. Ryan, S. M. Carbotte, B. M. Muhlenkamp, and W. F. Haxby (2003), Constraints on asthenospheric flow from the depth of oceanic spreading centers, *Eos Trans. AGU*, *84*(46), Fall Meet. Suppl., Abstract T52E–06.
Campbell, I. H., and R. W. Griffiths (1990), Implications of mantle plume structure for the evolution of flood basalts, *Earth Planet. Sci. Lett.*, *99*, 79–93, doi:10.1016/0012-821X(90)90072-6.
Chase, C. G. (1979), Asthenospheric counterflow: A kinematic model, *Geophys. J. R. Astron. Soc.*, *56*, 1–18.
Chen, Y. J. (1992), Oceanic crustal thickness versus spreading rate, *Geophys. Res. Lett.*, *19*, 753–756, doi:10.1029/92GL00161.
Christie, D. M., B. P. West, D. G. Pyle, and B. B. Hanan (1998), Chaotic topography, mantle flow and mantle migration in the Australian-Antarctic discordance, *Nature*, *394*, 637–644, doi:10.1038/29226.
Christie, D. M., D. G. Pyle, R. B. Pedersen, and D. J. Miller (2004), Leg 187 synthesis: Evolution of the Australian Antarctic Discordance, the Australian Antarctic depth anomaly, and the Indian/Pacific mantle isotopic boundary [online], *Proc. Ocean Drill. Program Sci. Results, 187*, 18 pp. (Available at http://www-odp.tamu.edu/publications/187_SR/synth/synth.htm)
Cochran, J. R., J. C. Sempere, and SEIR-Scientific-Team (1997), The Southeast Indian Ridge between 88°E and 120°E: Gravity anomalies and crustal accretion at intermediate spreading rates, *J. Geophys. Res.*, *102*, 15,463–15,487, doi:10.1029/97JB00511.
Courtillot, V., A. Davaille, J. Besse, and J. Stock (2003), Three distinct types of hotspots in the Earth's mantle, *Earth Planet. Sci. Lett.*, *205*, 295–308, doi:10.1016/S0012-821X(02)01048-8.
Crough, S. T. (1978), Thermal origin of mid-plate hot-spot swells, *Geophys. J. R. Astron. Soc.*, *55*, 451–469.
Davies, G. F. (1999), *Dynamic Earth: Plates, Plumes and Mantle Convection*, 398 pp., Cambridge Univ. Press, Cambridge, U. K.
DeMets, C., R. G. Gordon, D. F. Argus, and S. Stein (1994), Effects of recent revisions of the geomagnetic reversal time scale on estimates of current plate motions, *Geophys. Res. Lett.*, *21*, 2191–2194, doi:10.1029/94GL02118.
Detrick, R. S., and S. T. Crough (1978), Island subsidence, hot spots, and lithospheric thinning, *J. Geophys. Res.*, *83*, 1236–1244, doi:10.1029/JB083iB03p01236.
Forsyth, D. W., R. L. Ehrenbard, and S. Chapin (1987), Anomalous upper mantle beneath the Australian-Antarctic discordance, *Earth Planet. Sci. Lett.*, *84*, 471–478, doi:10.1016/0012-821X(87)90011-2.
Forsyth, D. W., et al. (1998), Imaging the deep seismic structure beneath a mid-ocean ridge: The MELT experiment, *Science*, *280*, 1215–1218, doi:10.1126/science.280.5367.1215.
Foulger, G. R., and D. L. Anderson (2005), A cool model for the Iceland hotspot, *J. Volcanol. Geotherm. Res.*, *141*, 1–22, doi:10.1016/j.jvolgeores.2004.10.007.
Gripp, A. E., and R. G. Gordon (1990), Current plate velocities relative to the hotspots incorporating the NUVEL-1 global plate motion model, *Geophys. Res. Lett.*, *17*, 1109–1112, doi:10.1029/GL017i008p01109.
Gurnis, M., and R. D. Müller (2003), Origin of the Australian Antarctic Discordance from an ancient slab and mantle wedge, in *Evolution and Dynamics of the Australian Plate*, edited by R. R. Hillis and R. D. Müller, *Spec. Publ. Geol. Soc. Aust.*, *22*, 417–429.
Gurnis, M., R. D. Müller, and L. Moresi (1998), Dynamics of Cretaceous vertical motion of Australia and the Australian-Antarctic discordance, *Science*, *279*, 1499–1504, doi:10.1126/science.279.5356.1499.
Haxby, W. F., and J. K. Weissel (1986), Evidence for small-scale mantle convection from seasat altimeter data, *J. Geophys. Res.*, *91*, 3507–3520, doi:10.1029/JB091iB03p03507.
Hill, R. I. (1991), Starting plumes and continental breakup, *Earth Planet. Sci. Lett.*, *104*, 398–416, doi:10.1016/0012-821X(91)90218-7.
Hirth, G., and D. L. Kohlstedt (1996), Water in the oceanic upper mantle: Implications for rheology, melt extraction and evolution of the lithosphere, *Earth Planet. Sci. Lett.*, *144*, 93–108, doi:10.1016/0012-821X(96)00154-9.
Holmes, R., M. Tolstoy, A. J. Harding, and J. A. Orcutt (2008), Crustal structure of the Southeast Indian Ridge at the eastern boundary of the Australian-Antarctic Discordance from seismic refraction data, *Eos Trans. AGU*, *89*(53), Fall Meet. Suppl., Abstract V41B-2086.
Huang, J., and S. Zhong (2005), Sublithospheric small-scale convection and its implications for the residual topography at old ocean basins and the plate model, *J. Geophys. Res.*, *110*, B05404, doi:10.1029/2004JB003153.
Ito, G., J. Lin, and C. W. Gable (1996), Dynamics of mantle flow and melting at a ridge-centered hotspot: Iceland and the Mid-Atlantic Ridge, *Earth Planet. Sci. Lett.*, *144*, 53–74, doi:10.1016/0012-821X(96)00151-3.
Jordan, T. H. (1981), Continents as a chemical boundary layer, *Philos. Trans. R. Soc. London, Ser. A*, *301*, 359–373, doi:10.1098/rsta.1981.0117.
King, S. D. (1995), Models of mantle viscosity, in *Mineral Physics and Crystallography: A Handbook of Physical Constants*, *AGU Ref. Shelf*, vol. 2, edited by T. J. Ahrens, pp. 227–236, AGU, Washington, D. C.
King, S. D., and G. Masters (1992), An inversion for radial viscosity structure using seismic tomography, *Geophys. Res. Lett.*, *19*, 1551–1554, doi:10.1029/92GL01700.
Kingsley, R. H., and J. G. Schilling (1998), Plume-ridge interaction in the Easter-Salas y Gomez seamount chain-Easter microplate system: Pb isotope evidence, *J. Geophys. Res.*, *103*, 24,159–24,177, doi:10.1029/98JB01496.
Kirby, S. H. (1983), Rheology of the lithosphere, *Rev. Geophys.*, *21*, 1458–1487, doi:10.1029/RG021i006p01458.

Klein, E. M., and C. H. Langmuir (1987), Global correlations of ocean ridge basalt chemistry with axial depth and crustal thickness, *J. Geophys. Res.*, *92*, 8089–8115, doi:10.1029/JB092iB08p08089.

Klein, E. M., C. H. Langmuir, A. Zindler, H. Staudigel, and B. Hamelin (1988), Isotope evidence of a mantle convection boundary at the Australian-Antarctic Discordance, *Nature*, *333*, 623–629, doi:10.1038/333623a0.

Lambeck, K., C. Smither, and P. Johnston (1998), Sea-level change, glacial rebound and mantle viscosity for northern Europe, *Geophys. J. Int.*, *134*, 102–144, doi:10.1046/j.1365-246x.1998.00541.x.

Lin, S.-C., L.-Y. Chiao, and B.-Y. Kuo (2002), Dynamic interaction of cold anomalies with the mid-ocean ridge flow field and its implications for the Australian-Antarctic discordance, *Earth Planet. Sci. Lett.*, *203*, 925–935, doi:10.1016/S0012-821X(02)00948-2.

Marks, K. M., P. R. Vogt, and S. A. Hall (1990), Residual depth anomalies and the origin of the Australian-Antarctic discordance zone, *J. Geophys. Res.*, *95*, 17,325–17,337, doi:10.1029/JB095iB11p17325.

Marks, K. M., D. T. Sandwell, P. R. Vogt, and S. A. Hall (1991), Mantle downwelling beneath the Australian-Antarctic discordance zone: Evidence from geoid height versus topography, *Earth Planet. Sci. Lett.*, *103*, 325–338, doi:10.1016/0012-821X(91)90170-M.

Marks, K. M., J. M. Stock, and K. J. Quinn (1999), Evolution of the Australian-Antarctic discordance since Miocene time, *J. Geophys. Res.*, *104*, 4967–4981, doi:10.1029/1998JB900075.

McNutt, M. K. (1998), Superswells, *Rev. Geophys.*, *36*, 211–244, doi:10.1029/98RG00255.

Medvedev, S. (2002), Mechanics of viscous wedges: Modeling by analytical and numerical approaches, *J. Geophys. Res.*, *107*(B6), 2123, doi:10.1029/2001JB000145.

Molnar, P., and J. M. Stock (1987), Relative motions of hotspots in the Pacific, Atlantic and Indian oceans since late Cretaceous time, *Nature*, *327*, 587–591, doi:10.1038/327587a0.

Morgan, W. J. (1971), Convection plumes in the lower mantle, *Nature*, *230*, 42–43, doi:10.1038/230042a0.

Morgan, W. J. (1972a), Deep mantle convection plumes and plate motions, *Bull. Am. Assoc. Pet. Geol.*, *56*, 203–213.

Morgan, W. J. (1972b), Plate motions and deep mantle convection, in *Studies in Earth and Space Sciences*, *Mem. Geol. Soc. Am.*, *132*, 7–22.

Müller, R. D., J. Y. Royer, and L. A. Lawver (1993), Revised plate motions relative to the hotspots from combined Atlantic and Indian Ocean hotspot tracks, *Geology*, *21*, 275–278, doi:10.1130/0091-7613(1993)021<0275:RPMRTT>2.3.CO;2.

Müller, R. D., C. Gaina, and S. Clarke (2000), Seafloor spreading around Australia, in *Billion-Year Earth History of Australia and Neighbours in Gondwanaland*, edited by J. Veevers, pp. 18–28, Gemoc, Sydney, N. S. W., Australia.

Nagel, T. J., W. B. F. Ryan, A. Malinverno, and W. R. Buck (2008), Pacific trench motions controlled by the asymmetric plate configuration, *Tectonics*, *27*, TC3005, doi:10.1029/2007TC002183.

Nettles, M., and A. M. Dziewoński (2008), Radially anisotropic shear velocity structure of the upper mantle globally and beneath North America, *J. Geophys. Res.*, *113*, B02303, doi:10.1029/2006JB004819.

Nishimura, C. E., and D. W. Forsyth (1985), Anomalous Love wave phase velocities in the Pacific: Application of a new method for joint pure-path and spherical harmonic inversion, *Geophys. J. R. Astron. Soc.*, *81*, 389–407.

Oxburgh, E. R., and E. M. Parmentier (1977), Compositional and density stratification in oceanic lithosphere: Causes and consequences, *J. Geol. Soc.*, *133*, 343–355, doi:10.1144/gsjgs.133.4.0343.

Parmentier, E. M., and J. E. Oliver (1979), A study of shallow global mantle flow due to the accretion and subduction of lithospheric plates, *Geophys. J. Int.*, *57*, 1–21, doi:10.1111/j.1365-246X.1979.tb03768.x.

Parsons, B., and J. G. Sclater (1977), Ocean floor bathymetry and heat flow, *J. Geophys. Res.*, *82*, 803–827, doi:10.1029/JB082i005p00803.

Paterson, W. S. B. (1994), *The Physics of Glaciers*, 480 pp., Pergamon, Oxford, U. K.

Phipps Morgan, J. (1997), The generation of a compositional lithosphere by mid-ocean ridge melting and its effect on subsequent off-axis hotspot upwelling and melting, *Earth Planet. Sci. Lett.*, *146*, 213–232, doi:10.1016/S0012-821X(96)00207-5.

Phipps Morgan, J., and W. H. F. Smith (1992), Flattening of the seafloor depth-age curve as a response to asthenospheric flow, *Nature*, *359*, 524–527, doi:10.1038/359524a0.

Phipps Morgan, J., W. J. Morgan, Y. Zhang, and W. H. F. Smith (1995), Observational hints for a plume-fed, suboceanic asthenosphere and its role in mantle convection, *J. Geophys. Res.*, *100*, 12,753–12,767.

Ribe, N. M., and U. Christensen (1994), Three-dimensional modeling of a mantle plume interacting with a moving lithospheric plate, *J. Geophys. Res.*, *99*, 669–682, doi:10.1029/93JB02386.

Richards, M. A., and B. H. Hager (1984), Geoid anomalies in a dynamic Earth, *J. Geophys. Res.*, *89*, 5987–6002, doi:10.1029/JB089iB07p05987.

Richter, F. M., and B. Parsons (1975), On the interaction of two scales of convection in the mantle, *J. Geophys. Res.*, *80*, 2529–2541, doi:10.1029/JB080i017p02529.

Ritzwoller, M. H., N. M. Shapiro, A. L. Levshin, and G. M. Leahy (2001), Crustal and upper mantle structure beneath Antarctica and surrounding oceans, *J. Geophys. Res.*, *106*, 30,645–30,670, doi:10.1029/2001JB000179.

Ritzwoller, M. H., N. M. Shapiro, and G. M. Leahy (2003), A resolved mantle anomaly as the cause of the Australian-Antarctic Discordance, *J. Geophys. Res.*, *108*(B12), 2559, doi:10.1029/2003JB002522.

Ryan, W. B. F., B. M. Muhlenkamp, W. F. Haxby, S. M. Carbotte, and W. R. Buck (2003), Deep continental lithosphere keels as impediments to asthenosphere flow and cause of ocean crust depth anomalies, *Eos Trans. AGU*, *84*(46), Fall Meet. Suppl., Abstract T52E–05.

Schilling, J. G. (1991), Fluxes and excess temperatures of mantle plumes inferred from their interaction with migrating mid-ocean ridges, *Nature*, *352*, 397–403, doi:10.1038/352397a0.

Schubert, G., and D. L. Turcotte (1972), One-dimensional model of shallow-mantle convection, *J. Geophys. Res.*, *77*, 945–951, doi:10.1029/JB077i005p00945.

Simons, F. J., A. Zielhuis, and R. D. van der Hilst (1999), The deep structure of the Australian continent from surface wave tomography, *Lithos*, *48*, 17–43, doi:10.1016/S0024-4937(99)00041-9.

Sleep, N. (1990), Hotspots and mantle plumes: Some phenomenology, *J. Geophys. Res.*, *95*, 6715–6736, doi:10.1029/JB095iB05p06715.

Sleep, N. H. (1996), Lateral flow of hot plume material ponded at sublithospheric depths, *J. Geophys. Res.*, *101*, 28,065–28,083, doi:10.1029/96JB02463.

Sleep, N. H. (2006), Mantle plumes from top to bottom, *Earth Sci. Rev.*, *77*, 231–271, doi:10.1016/j.earscirev.2006.03.007.

Small, C. (1998), Global systematics of mid-ocean ridge morphology, in *Faulting and Magmatism at Mid-Ocean Ridges*, *Geophys. Monogr. Ser.*, vol. 106, edited by W. R. Buck et al., pp. 1–25, AGU, Washington, D. C.

Small, C., and L. Danyushevsky (2003), A plate kinematic explanation for mid-ocean ridge depth discontinuities, *Geology*, *31*, 399–402, doi:10.1130/0091-7613(2003)031<0399:PEFMDD>2.0.CO;2.

Stein, C. A., and S. Stein (1992), A model for the global variation in oceanic depth and heat flow with lithospheric age, *Nature*, *359*, 123–129, doi:10.1038/359123a0.

Stock, J. M., and P. Molnar (1983), Some geometrical aspects of uncertainties in combined plate reconstructions, *Geology*, *11*, 697–701, doi:10.1130/0091-7613(1983)11<697:SGAOUI>2.0.CO;2.

Tolstoy, M., J. A. Orcutt, and J. Phipps Morgan (1995), Crustal thickness at the Australian-Antarctic Discordance and neighboring South East Indian ridge, *Eos, Trans. AGU*, *76*, 570.

Turcotte, D., and G. Schubert (2002), *Geodynamics*, 456 pp., Cambridge Univ. Press, New York.

Veevers, J. J. (1986), Breakup of Australia and Antarctica estimated as mid-Cretaceous (95 ± 5 Ma) from magnetic and seismic data at the continental margin, *Earth Planet. Sci. Lett.*, *77*, 91–99, doi:10.1016/0012-821X(86)90135-4.

Vogt, P. R. (1971), Asthenosphere motion recorded by the ocean floor south of Iceland, *Earth Planet. Sci. Lett.*, *13*, 153–160, doi:10.1016/0012-821X(71)90118-X.

Vogt, P. R. (1976), Plumes, subaxial pipe flow and topography along the mid-oceanic ridge, *Earth Planet. Sci. Lett.*, *29*, 309–325, doi:10.1016/0012-821X(76)90135-7.

Vogt, P. R., N. Z. Cherkis, and G. A. Morgan (1983), Projector Investigator-I: Evolution of the Australian–Antarctic Discordance deduced from a detailed aeromagnetic study, in *Antarctic Earth Science: Proceedings of the Fourth International Symposium on Antarctic Earth Sciences, Held at University of Adelaide, South Australia, 16 to 20 August 1982*, edited by R. L. Oliver, P. R. James, and J. B. Jago, pp. 608–613, Aust. Acad. of Sci., Canberra, A.C.T., Australia.

Weissel, J. K., and D. E. Hayes (1974), The Australian-Antarctic Discordance: New results and implications, *J. Geophys. Res.*, *79*, 2579–2587, doi:10.1029/JB079i017p02579.

West, B. P., J. C. Sempere, D. G. Pyle, J. Phipps Morgan, and D. M. Christie (1994), Evidence for variable upper mantle temperature and crustal thickness in and near the Australian-Antarctic Discordance, *Earth Planet. Sci. Lett.*, *128*, 135–153, doi:10.1016/0012-821X(94)90141-4.

West, B. P., W. S. D. Wilcock, and J.-C. Sempere (1997), Three-dimensional structure of asthenospheric flow beneath the Southeast Indian Ridge, *J. Geophys. Res.*, *102*, 7783–7802, doi:10.1029/96JB03895.

Yale, M., and J. Phipps Morgan (1998), Asthenosphere flow model of hotspot-ridge interactions: A comparison of Iceland and Kerguelen, *Earth Planet. Sci. Lett.*, *161*, 45–56, doi:10.1016/S0012-821X(98)00136-8.